On the Dynamics of Droughts in Northeast Brazil: Observations, Theory and Numerical Experiments with a General Circulation Model

ANTONIO D. MOURA[1]

Instituto de Pesquisas Espaciais, CNPq/INPE, Sao Jose dos Campos, Sao Paulo, Brazil

JAGADISH SHUKLA

Goddard Laboratory for Atmospheric Sciences, NASA/GSFC, Greenbelt, MD 20771

(Manuscript received 8 June 1981, in final form 13 August 1981)

ABSTRACT

It is proposed that a possible mechanism for the occurrence of severe droughts over northeast Brazil is the establishment of a thermally direct local circulation which has its ascending branch at about 10°N and its descending branch over northeast Brazil and the adjoining oceanic region. The driving for this anomalous circulation is provided by warming due to enhanced moist convection associated with warmer sea surface temperature anomalies over the northern tropical Atlantic, and cooling associated with colder sea surface temperature anomalies in the southern tropical Atlantic. The combined effects of thermally forced subsidence and reduced evaporation and moisture flux convergence produces severe drought conditions over northeast Brazil.

We have examined the monthly mean sea surface temperature anomalies over the tropical Atlantic and rainfall anomalies over two selected stations (Fortaleza, 3°46'S 38°31'W and Quixeramobim, 5°12'S 39°18'W) for 25 years (1948–72). It is found that the most severe drought events are associated with the simultaneous occurrence of warm sea surface temperature anomalies over north and cold sea surface temperature anomalies over the south tropical Atlantic. Simultaneous occurrences of warm sea surface temperature anomaly at 15°N, 45°W and cold sea surface temperature anomaly at 15°S, 5°W were *always* associated with negative anomalies of rainfall, and vice versa.

A simple primitive equation model is used to calculate the frictionally controlled and thermally driven circulation due to a prescribed heating function in a resting atmosphere. The heating function is designed to simulate a heat source to the north and a heat sink to the south of the equator. This prescribed thermal forcing produces a thermally direct circulation with ascending motion to the north and descending motion to the south. Low-level cyclonic circulation and high-level anticyclonic circulation is generated to the north of the equator and low-level anticylonic circulation and high-level cyclonic circulation is generated to the south of the equator. The analytical solutions agree well with the results of numerical experiments carried out with a multilevel global general circulation model.

We also have carried out a series of numerical experiments to test the sensitivity of the GLAS (Goddard Laboratory for Atmospheric Sciences) model to prescribed sea surface temperature anomalies over the tropical Atlantic. It is found that the sea surface temperature anomaly patterns, which resemble the observed ones during drought years, produce an intensified convergence zone, enhanced rainfall and low-level cyclonic circulation to the north, and reduced rainfall and anticyclonic circulation to the south. The reduction of rainfall over continental northeast Brazil is large enough to give further support to the proposed mechanism.

Since the sea surface temperature anomalies over the tropical Atlantic persist for several months, the proposed mechanism could provide guidance for predicting droughts over northeast Brazil.

1. Introduction

The mean rainfall over northeast Brazil and its interannual variability constitute one of the most challenging yet unsolved problems of tropical meteorology. Due to its geography (1–18°S, 35–47°W), one would expect a rainfall distribution typical of equatorial areas. However, the annual mean rainfall over this region, which is in the immediate vicinity of the largest tropical forest, the Amazon, is much smaller than the average equatorial rainfall (Fig. 1). The region is known to have one of the "earth's problem climates" (Trewartha, 1961; Ratisbona, 1976; Riehl, 1979). The mean annual rainfall is less than 800 mm in most of the area, lowering to 500 mm in its interior (Kousky and Chu, 1978), and the rainfall amount exceeds 0.1 mm for only 60 days of the year (Ratisbona, 1976).

In the northern and central part of the northeast

[1] This work was performed during a visit to Goddard Laboratory for Atmospheric Sciences, GSFC/NASA.

0022-4928/81/122653-23$09.75

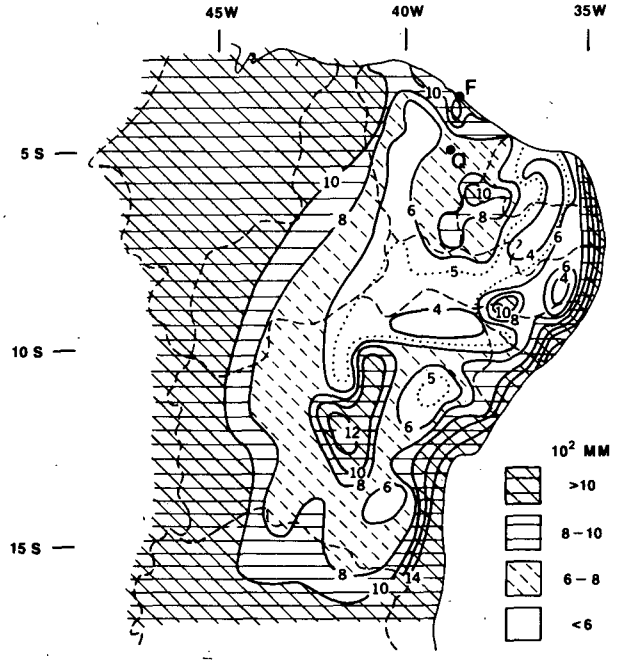

FIG. 1. Annual mean precipitation (10^2 mm) over Northeast Brazil (from Kousky and Chu, 1978).

Brazil region, the seasonal distribution of rainfall shows a sharp peak for March–April (Henry, 1922; Aldaz, 1971; Strang, 1972), when the Intertropical Convergence Zone (ITCZ) is in its extreme southerly position (Ratisbona, 1976). The influence of the ITCZ displacement on the regional rainfall has been shown by Serra and Ratisbona (1942) and more recently by Hastenrath and Heller (1977).

The southern part receives its maximum precipitation from November to March with a peak in December. This region is under the influence of equatorward excursions of cold fronts as suggested by Sampaio Ferraz (1925, 1929), Ratisbona (1976), and has been recently well documented by Kousky (1979).

On the east coast, the mean flow and land-sea breeze influence is such that rainfall shows a nocturnal maximum along the coast and daytime maximum far inland up to 300 km (Kousky, 1980; Ramos, 1975). The coastal precipitation is also influenced by westward propagating cloud clusters during May–July, as shown by Yamazaki and Rao (1977).

It can be argued that the existence of this semiarid climate is due to the fact that the region is in the vicinity of the trade wind inversion and also, because of its geography, the tip of northeast Brazil (alternately referred to as the Northeast) protrudes well into the area of permanent influence of the semipermanent South Atlantic subtropical high. In addition, local effects of topography and differential albedo also seem to be important. For example, Charney's (1975) explanation for self-maintenance of a desert region has been shown to be applicable for this region by Gomes Filho (1979).

The impact of climate fluctuations on the social and economic life of the local population (more than 30 million) is enormous (Cunha, 1940; Marinho and Reboucas, 1971; Rose, 1980). This is mainly because of the large year-to-year variation of total rainfall [the variability is greater than 40% in some interior areas (Kousky, 1979)], with the occurrence of extreme droughts and also floods in some years. Table 1 shows the years of major droughts. A comprehensive evaluation of proposed methods for predicting droughts in the Northeast appears in a report edited by Carvalho (1973). More recently, the Brazilian National Research Council (CNPq) has reviewed several facets of the problem of the climate of this region and its variability (Smagorinsky *et al.*, 1980).

The relationship between frequency of sun spot minima and droughts has been studied by Derby (1885) and Hull (1942). Sampaio Ferraz (1950) even issued drought forecasts based on the sun spot cycle. Rainfall time series for Fortaleza (3°46′S, 38°31′W), Ceara, which began in 1849, has been analyzed by Markham (1974) and also by Strang (1979) who found significant periods of 13 and 26 years. Jones and Kearns (1976) have questioned the statistical significance of Markham's findings.

Mossman (1919) indicated that the causes of drought in the Northeast seemed to be global. Walker (1928) suggested a possible relationship between the Southern Oscillation and rainfall over the Northeast, but he did not feel confident to issue forecasts even though two-thirds of the droughts could have been foretold correctly by his formula with the data available at that time. Extending Walker's ideas, Serra (1945, 1956, 1973a,b,c) has extensively studied the relationship between rainfall variability in the Northeast and the "World's Weather". Namias (1972) showed a relationship between the interannual variation of rainfall at Quixeramobim (5°12′S, 39°18′W) and the cyclonic activity near

TABLE 1. Years of major droughts in northeast Brazil. Asterisks indicate years of extreme droughts. (Sources: Mossman 1919; Sampaio Ferraz, 1950; Hastenrath and Heller, 1977).

1603	1711	1804	1900*
1614*	1721	1809	1902–03
1692	1723–24*	1810	1907
	1736–37	1816–17	1915*
	1744–46	1824–25*	1919*
	1754	1827	1932–33
	1760	1830–33	1936
	1772	1845	1941–44*
	1776–77*	1877–79*	1951
	1784	1888–89	1953
	1790–94*	1891	1958*
		1898	1980

Newfoundland during winter and spring of the Northern Hemisphere. Caviedes (1973) finds that drought in the Northeast is a simultaneous event with the occurrence of El Niño off the Ecuador–Peru coast. It has thus been suggested that the two climatic hazards are linked to Walker's Southern Oscillation (Hastenrath and Heller, 1977; Covey and Hastenrath, 1978; Bjerknes, 1969). More recently, Hastenrath and Heller (1977) have shown strong evidence that the seasonal displacement of the circulation complex comprised by the low-pressure trough embedded in the North Atlantic confluence axis between the North and South Atlantic highs seems to explain the rainfall variability in the northern part of northeast Brazil. They show that dry years are characterized by a northward displacement of both subtropical Atlantic highs.

Observational evidence of a possible relationship between sea surface temperature (SST) anomalies over the Atlantic and rainfall over Northeast Brazil has been presented by Markham and McLain (1977) and Hastenrath and Heller (1977). Markham and McLain (1977) correlated December SST, over the South Atlantic area west of Africa, with January, February and March rainfall at Fortaleza and Quixeramobim, explaining half of Ceara's rainfall variance. Hastenrath and Heller (1977) and Hastenrath (1978) show that in years of droughts, SST anomalies in the tropical Atlantic display a pattern of positive values to the north and negative values to the south of equator. For wet years the pattern is essentially reversed. They have pointed out an inverse relationship between the rainfall over northeast Brazil and Guyana. This relationship is attributed to the northward displacement of the ITCZ. Since the locations of the ITCZ during dry and wet years are not different by more than 2–3° of latitude, it is not clear if the convergence zone as defined by Hastenrath and Heller (1977) is a critical determinant of droughts over the Northeast.

The observational evidence presented by Hastenrath and Heller (1977) and Markham and McLain (1977) leads us to postulate that a possible dynamical mechanism responsible for the occurrence of droughts over northeast Brazil is the simultaneous existence of a heat source to the north and a cold sink to the south of the equator. The localized dynamical circulation associated with such a thermal forcing will produce ascending motion and low-level cyclonic vorticity to the north and descending motion and low-level divergence to the south over the Northeast and its adjoining oceanic region. Since the tropical SST anomalies and the associated moist convective processes provide an efficient mechanism to generate vertically distributed heat sources, we examined the distribution of SST anomalies over tropical Atlantic for the 25-year period (1948–72), originally prepared by Bunker (1976). We were struck by the consistency of SST anomaly patterns in relation to extreme precipitation regimes over the Northeast. For example, during the three major drought years of 1951, 1953 and 1958 warm SST anomalies occurred to the north and cold SST anomalies to the south of the equator. It was observed and later verified by numerical experiments with the GLAS model, that the warm SST anomalies over the oceanic region around 15°N, 45°W were more effective than the anomalies further east near the African coast in determining the low precipitation regime over northeast Brazil. The SST anomaly pattern chosen by Rowntree (1976) is not related to droughts over northeast Brazil because the warmest anomaly occurs off the African coast where the climatological mean temperature of the ocean is relatively low. The spatial structure and the location of SST anomalies seem to be an important factor in determining its impact on the precipitation over the Northeast. In the next section we present the observations of SST anomalies and their relationships to rainfall at selected stations in northeast Brazil.

In Section 3, we present the results of an analytical study in which we have used a simplified form of the linearized primitive equations for a resting atmosphere to calculate the response to a prescribed thermal forcing that can be produced by simultaneous existence of a warm SST anomaly and enhanced moist convection to the north and a cold SST anomaly to the south of the equator. The analytical results show a thermally direct circulation with ascent over the region of heating and descent over the region of cooling. Although the model is extremely simple, it provides a good physical insight to interpret the results of a more complex general circulation model.

In Section 4, we present the results of a series of numerical experiments carried out to test the sensitivity of the GLAS model to prescribed SST anomaly patterns. The results of these experiments are in agreement with the observations and provide further support to the validity of the proposed mechanism for droughts over northeast Brazil. Since the SST anomalies persist for several months, there seems to be some potential for predicting droughts over northeast Brazil.

2. Observational evidence of relationship between SST anomaly and rainfall

Hastenrath and Heller (1977) studied 60 years of SST anomalies over the tropical Atlantic and their relationship with annual rainfall over northeast Brazil. They presented composite charts of SST anomalies for 10 extreme dry years and 10 extreme wet years during the period studied (1912–72). For the ten driest years in northeast Brazil, the com-

TABLE 2. Monthly mean (1849–1978) precipitation (mm) for Fortaleza and Quixeramobim (Namias, 1972).

Month	Fortaleza 3°46'S, 38°31'W	Quixeramobim 5°12'S, 39°18'W
Jan	92	43
Feb	185	88
Mar	299	171
Apr	336	160
May	234	102
Jun	117	39
Jul	57	20
Aug	23	9
Sept	18	4
Oct	15	3
Nov	17	6
Dec	37	16
Total	1430	661

posite chart of March and April mean SST anomalies shows a large area of positive departures northward of the equator up to 30°N from Africa to the Caribbean region, and an area of negative departures southward of the equator extending from Africa to northeast Brazil. For the ten extreme wet years the chart of composite SST anomalies shows a pattern which is essentially the reserve, with warm SST anomalies to the south and cold SST anomalies to the north of the equator. This latter pattern resembles the third SST principal component calculated by Hastenrath (1978).

Markham and McLain (1977) have calculated the correlation between mean monthly SST anomalies, over 5° latitude-longitude quadrants in the South Atlantic, and the January, February, March rainfall for Fortaleza and Quixeramobim. For the period 1947–67, their correlation maps show a westward displacement of the area of higher correlation, beginning in November, increasing in December and disappearing in April. Based on this, Markham and McLain (1977) established a correlation formula for predicting rainfall over northeast Brazil, given December SST in the selected 5° × 5° square (7.5°S, 2.5°W) where the correlation is highest. Their explanation for the high correlation is that a warm SST anomaly over the equatorial South Atlantic deepens the moist layer and increases rainfall, while a cold SST anomaly decreases wind flow and reduces convection over northeast Brazil. The results of Markham and McLain (1977) are quite consistent with other studies on relationships between tropical SST anomalies and rainfall. For example, Shukla and Misra (1977) found a positive correlation between SST anomalies over the Arabian Sea and rainfall over the Indian monsoon area. They also found an inverse relationship between SST anomalies and wind strength, which was noted by Markham and McLain (1977) for the South Atlantic.

In the present study, we have used 25 years of SST data (averaged over 10° latitude-longitude squares) for the period 1948–72 (Bunker, 1976) over both the South and North Atlantic to calculate the correlation between March SST anomalies and mean rainfall for March, April and May at Fortaleza and Quixeramobim. Table 2 gives the monthly mean precipitation at these two stations. The precipitation shows a pronounced peak for the 3-month period of March, April, May, which represent more than 62% of the total precipitation. Fig. 2 shows the rainfall

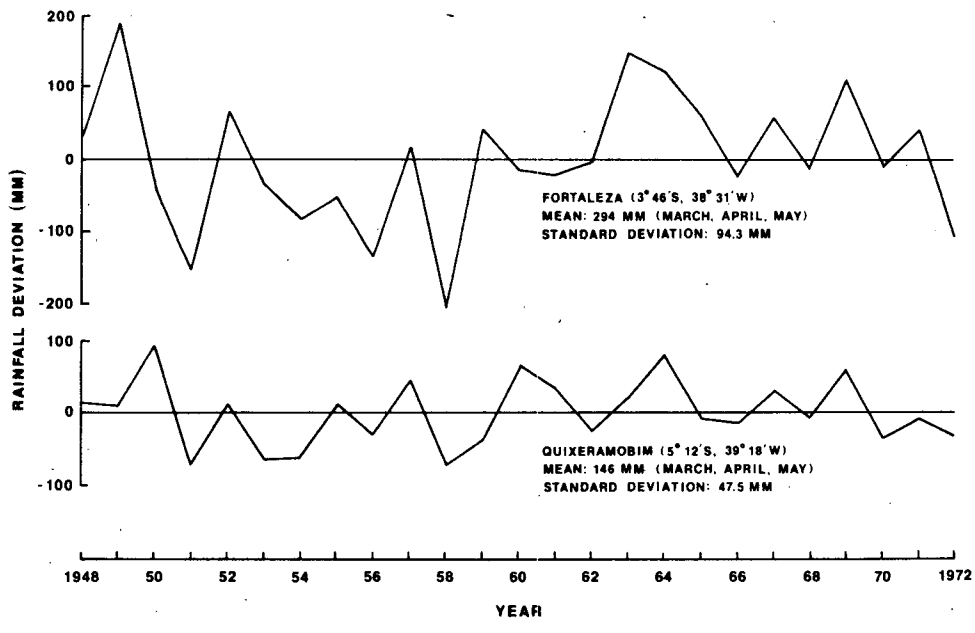

FIG. 2. Average rainfall departures for March, April, May at Fortaleza and Quixeramobim.

time series for Fortaleza and Quixeramobin. The mean and standard deviation of Fortaleza's rainfall is twice that of Quixeramobin.

The correlation between March SST anomalies and normalized rainfall departures for the tropical North and South Atlantic is shown in Fig. 3. In the South Atlantic, we find a large area of high positive correlation in agreement with Markham and McLain (1977). In the North Atlantic, however, we find a region around 15°N, 45°W with negative correlation values (values greater than 0.33 and 0.39 are significant at 90 and 95% confidence levels, respectively). Although this negative area in the North Atlantic is not as large as the positive area in the South Atlantic, we have found that it has a very important dynamical effect on the rainfall in northeast Brazil. The correlation coefficients presented in Fig. 3 are smaller than those found by Markham and McLain (1977). This is because we are using a longer time series (25 years) and SST is averaged over 10° latitude-longitude areas in contradistinction to Markham and McLain's 5° × 5° areas. We also are looking at SST anomalies and rainfall anomalies for different months.

The positive correlation found in the South Atlantic could be explained as follows: warm SST and increased evaporation over the ocean increase the moisture flux convergence and rainfall over the Northeast because the southeast trade winds flow directly toward northeast Brazil. On the other hand, cold SST decreases evaporation and reduces convection as indicated by Markham and McLain (1977). However, the major finding in the present study is that simultaneous occurrence of warm SST anomalies to the north and cold SST anomalies to the south reinforces the severe droughts over the northeast. This fact is illustrated in Fig. 4 which presents the 25-year rainfall deviations plotted as a function of SST anomaly in the 15°N, 45°W area (abscissa) and the mean of SST anomalies in the 15°S, 5°W and 5°S, 25°W areas (ordinate). These areas contain the highest correlation coefficients. It is striking that in the lower right quadrant of Fig. 4 all the rainfall departures are negative with the highest values being farthest away from the origin. In the upper left quadrant all rainfall departures are positive.

Looking at the actual monthly mean SST anomaly maps for extremely dry and extremely wet years in the Northeast, we find that the composite SST patterns of Hastenrath and Heller (1977) seem to appear also on an individual basis (droughts in 1951, 1953, 1958 and yet years in 1964, 1967). Since the mean sea surface temperature itself is quite warm (Hastenrath and Lamb, 1977) in the north, the SST anomalies are quite effective in producing a response in the atmosphere. An increased evaporation enhances deep convection in the ITCZ with ascending motion to the north and descending motion over northeast Brazil and the neighboring oceanic area. This local direct cell has a strong dynamical influence on the flow over the Northeast because it produces low-level divergence and reduces the regional rainfall. A possible reason for not finding large negative correlations to the north could be the dynamical nature of this relationship between SST anomaly

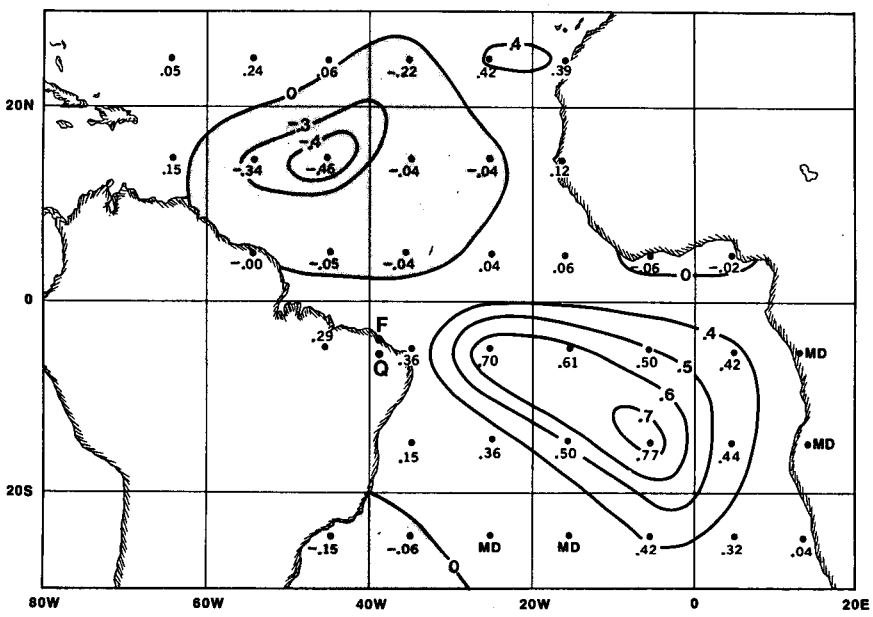

FIG. 3. Correlation coefficients between sea surface temperature over the Atlantic and average rainfall for Fortaleza and Quixeramobim.

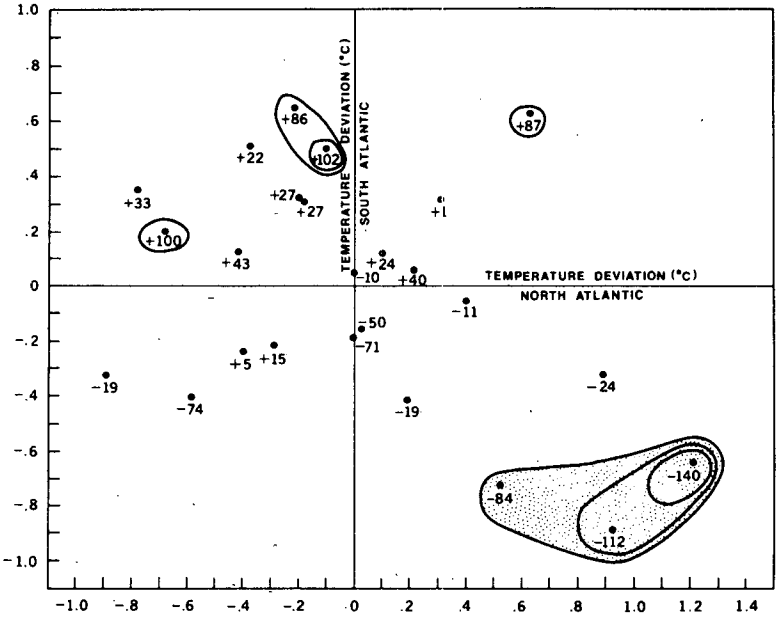

FIG. 4. Average of March, April, May rainfall departures (mm) at Fortaleza and Quixeramobim in relation to SST anomaly at 15°N, 45°W (abscissa) versus average of SST anomaly at 15°S, 5°W and 5°S, 25°W (ordinate).

and rainfall. Whereas a warmer SST produces an intense ITCZ and associated descending motion over the Northeast, a colder SST in the north does not necessarily induce rising motion and enhanced precipitation over the Northeast. Therefore, this relationship seems to be much stronger for severe drought events than compared to wet years.

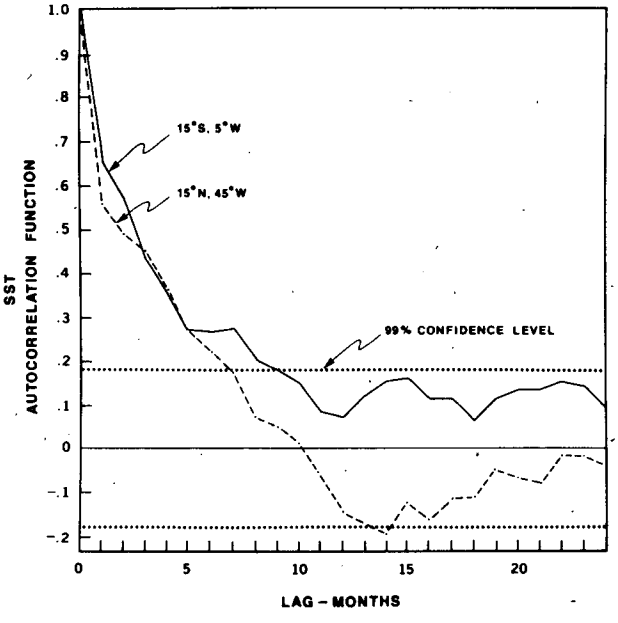

FIG. 5. Lag correlation function for monthly mean SST anomaly at 15°S, 5°W and 15°N, 45°W.

The autocorrelation functions for SST anomalies at 15°S, 5°W and at 15°N, 45°W are given in Fig. 5. The strong persistence of SST anomalies (above white noise at 99% confidence level for up to six months) in these two areas suggests a potential for prediction of drought occurrence in northeast Brazil. It is interesting to note (Fig. 5) that SST anomalies in the south (15°S, 5°W) are more persistent than in the north (15°N, 45°W).

3. A simple analytical study

This study is aimed at understanding the linearized, steady-state, equatorial atmospheric response to a prescribed distribution of diabatic heating associated with a SST anomaly.

a. The model equations

The linearized dynamics of hydrostatic, steady-state perturbations on a resting stratified atmosphere, in an equatorial beta plane, driven by differential heating and controlled by friction, can be written as

$$\epsilon u - yv = -\frac{\partial \phi}{\partial x}, \tag{1}$$

$$\epsilon v + yu = -\frac{\partial \phi}{\partial y}, \tag{2}$$

$$\frac{\partial \omega}{\partial p} = -\frac{\partial u}{\partial x} - \frac{\partial v}{\partial y}, \tag{3}$$

$$\omega = -\frac{p}{S(p)}\dot{q}. \tag{4}$$

These equations have been nondimensionalized (Pedlosky, 1979) by scaling the eastward and northward distances x and y by L; the pressure p by P ($=1000$ mb); the eastward and northward velocities u and v by V; the vertical velocity ω by (PV/L); the geopotential ϕ by $(\beta L^2 V)$; the constant Rayleigh friction ϵ by (βL); the diabatic heating by $(S_0/\kappa L)$; the static stability $S(p)$ by a typical value $S_0 = (H_0 N_0)^2$, where H_0 is the scale height and N_0 the Brunt–Väisällä frequency; $\beta = 2\Omega/a$ ($=2.28 \times 10^{-11}$ m^{-1} s^{-1}), $V \approx 10$ m s^{-1}). The length scale L is of the order of the equatorial Rossby radius of deformation [$L_R = (S_0/\beta^2)^{1/4}$] and is taken equal to 10^6 m, corresponding to the distance of maximum heating (near the ITCZ in the North Atlantic) from the equator.

The prescribed diabatic heating, which is an idealization of a warm SST anomaly to the north and a cold SST anomaly to the south, is assumed to be of the form

$$\dot{q}(x, y, p) = Q(p)X(x)Y(y). \tag{5}$$

The distributions of Q, X and Y are shown in Fig. 6. The function $Q(p)$ corresponds to a vertically distributed heating associated with the effective warm SST anomaly, which enhances deep convection near the ITCZ. The function $X(x)$ gives the east–west extent of the heating in the Atlantic and $Y(y)$ is taken positive and narrow to the north, and negative, weaker and broader to the south of equator. The functional form of $X(x)$ is taken as $e^{-x^2/2}$ and that of $Y(y)$ as $e^{-y^2/2}\sum_{n=0}^{4} a_n H_n(y)$, where the constants a_n are given in Fig. 6 and $H_i(y)$ is the ith-order Hermite polynomial.

The boundary conditions require the motions to be equatorially confined (i.e., the solutions decay for large $|y|$), and are bounded in the east-west directions. In the vertical, the mass flux is zero at the ground (taken flat) and at the top of the atmosphere. Thus, we will take $\omega = 0$ at the top and bottom of the atmosphere.

From (1)–(4) we can form an equation for v (the vorticity equation):

$$\epsilon\frac{\partial^2 v}{\partial y^2} + \epsilon\frac{\partial^2 v}{\partial x^2} + \frac{\partial v}{\partial x} = \left(\epsilon\frac{\partial}{\partial y} - y\frac{\partial}{\partial x}\right)\frac{\partial}{\partial p}\left(\frac{p}{S(p)}\dot{q}\right). \tag{6}$$

It can be seen that the solution of (6) is completely determined by the distribution of heating and the boundary conditions for v.

With the heating as given by (5), v admits solutions of the form

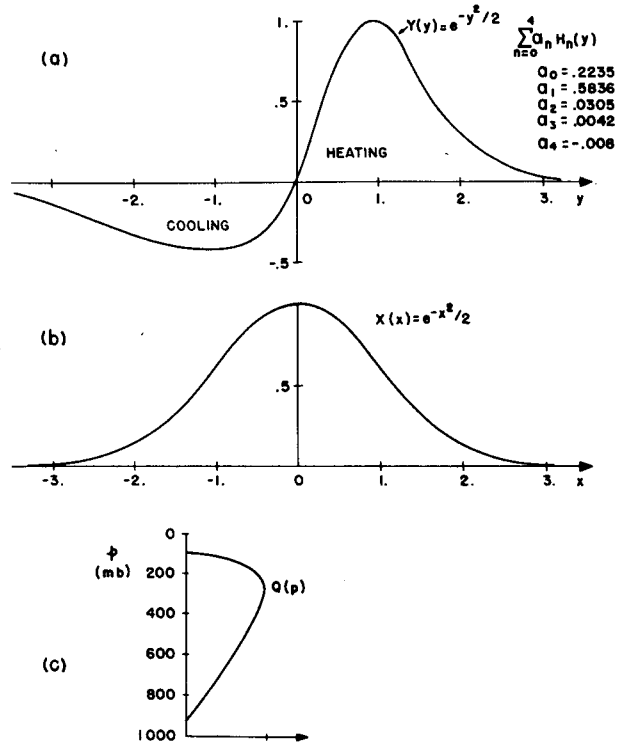

FIG. 6. X, Y and p structure of the prescribed diabatic heating function.

$$v(x, y, p) = A(p)V(y, x). \tag{7}$$

Then, Eqs. (6) and (7) give

$$A(p) = \frac{d}{dp}\left(\frac{p}{S(p)}Q(p)\right), \tag{8}$$

$$\epsilon\frac{\partial^2 V}{\partial y^2} + \epsilon\frac{\partial^2 V}{\partial x^2} + \frac{\partial V}{\partial x} = \epsilon X(x)\frac{dY}{dy} - yY(y)\frac{dX}{dx}. \tag{9}$$

The solution of (9) is found by expanding V in a series of Hermite functions which obey the boundary conditions $V \to 0$ as $|y| \to \infty$. Then

$$V(x, y) = \sum_{n=0}^{\infty} V_n(x)\psi_n(y), \tag{10}$$

where $\psi_n(y) = e^{-y^2/2}H_n(y)$ is the nth-order Hermite function, such that

$$\int_{-\infty}^{\infty} \psi_n\psi_m dy = \pi^{1/2}2^m m!\delta_{nm} \tag{11}$$

and

$$\frac{d^2\psi_n}{dy^2} = n(n-1)\psi_{n-2} - (n + \tfrac{1}{2})\psi_n + \tfrac{1}{4}\psi_{n+2}. \tag{12}$$

[Note: If time variation and a constant basic zonal advection are included in (1)–(4), one arrives at

$$E\frac{\partial^2 v}{\partial y^2} + E\frac{\partial^2 v}{\partial x^2} + \frac{\partial v}{\partial x} + \Lambda(E^2 + y^2)\frac{\partial}{\partial p}\left(\frac{pv}{S}\right) = \left(E\frac{\partial}{\partial y} - y\frac{\partial}{\partial x}\right)\frac{\partial}{\partial p}\left(\frac{p}{S}\dot{q}\right)$$

where

$$\Lambda \equiv \frac{\partial}{\partial t} + U\frac{\partial}{\partial x}, \quad E \equiv \frac{\partial}{\partial t} + U\frac{\partial}{\partial x} + \epsilon,$$

and U and t are the nondimensional zonal velocity advection and time, scaled by (βL^2) and (βL), respectively. The vertical structure of the solution will not simply separate as in (8), but, by taking solutions of the form $v(x, y, p, t) = \text{Re} \sum_k \times \sum_n e^{i(kx-\omega t)} V_n(y) A_n(p)$(Lindzen), 1967; Pedlosky, 1979), one has to solve an eigenvalue-eigenfunction problem to separate out the vertical and horizontal structures for the forced problem.]

Eq. (9) then becomes

$$\epsilon\frac{d^2 V_n}{dx^2} + \frac{dV_n}{dx} + \tfrac{1}{4}\epsilon V_{n-2} - \epsilon(n + \tfrac{1}{2})V_n + \epsilon(n + 1)(n + 2)V_{n+2} = \epsilon X F_n - \frac{dX}{dx} G_n, \quad (13)$$

with

$$\left.\begin{aligned} F_n &= \left[\int_{-\infty}^{\infty} \psi_n \frac{dY}{dy}\, dy\right](\pi^{1/2} 2^n n!)^{-1} \\ G_n &= \left[\int_{-\infty}^{\infty} Y Y \psi_n dy\right](\pi^{1/2} 2^n n!)^{-1} \end{aligned}\right\}. \quad (14)$$

Making a Fourier transformation of (13), by taking

$$\tilde{V}_n(k) = \frac{1}{\sqrt{2\pi}}\int_{-\infty}^{\infty} V_n e^{-ikx} dx,$$

$$\tfrac{1}{4}\epsilon\tilde{V}_{n-2} + [-\epsilon(n + \tfrac{1}{2}) - \epsilon k^2 + ik]\tilde{V}_n + \epsilon(n + 1)(n + 2)\tilde{V}_{n+2} = \epsilon\chi(k)F_n - D(k)G_n = \Theta_n, \quad (15)$$

where

$$\left.\begin{aligned} \chi(k) &= \frac{1}{\sqrt{2\pi}}\int_{-\infty}^{\infty} X(x) e^{-ikx} dx \\ D(k) &= \frac{1}{\sqrt{2\pi}}\int_{-\infty}^{\infty} \frac{dX}{dx} e^{-ikx} dx = ik\chi(k) \end{aligned}\right\}. \quad (16)$$

The system of equations (15) splits up into two symmetries and can be written, for $n = 0, 2, 4, \ldots,$ as

$$\begin{pmatrix} \epsilon\left(-\frac{1}{2} - k^2 + ik/\epsilon\right) & \epsilon(1.2) & 0 \cdots \\ \epsilon\left(\frac{1}{4}\right) & \epsilon\left(-\frac{5}{2} - k^2 + ik/\epsilon\right) & \epsilon(3.4) \quad 0 \cdots \\ 0 & \epsilon\left(\frac{1}{4}\right) & \epsilon\left(-\frac{9}{2} - k^2 + ik/\epsilon\right) \\ \vdots & 0 & \epsilon\left(\frac{1}{4}\right) \\ & \vdots & 0 \\ & & \vdots \end{pmatrix} \begin{pmatrix} \tilde{V}_0 \\ \tilde{V}_2 \\ \tilde{V}_4 \\ \vdots \end{pmatrix} = \begin{pmatrix} \Theta_0 \\ \Theta_2 \\ \Theta_4 \\ \vdots \end{pmatrix}. \quad (17)$$

and for $n = 1, 3, 5 \ldots$

$$\begin{pmatrix} \epsilon\left(-\frac{3}{2} - k^2 + ik/\epsilon\right) & \epsilon(2.3) & 0 \cdots \\ \epsilon\left(\frac{1}{4}\right) & \epsilon\left(-\frac{7}{2} - k^2 + ik/\epsilon\right) & \epsilon(4.5) \quad 0 \cdots \\ 0 & \epsilon\left(\frac{1}{4}\right) & \\ \vdots & 0 & \\ & \vdots & \end{pmatrix} \begin{pmatrix} \tilde{V}_1 \\ \tilde{V}_3 \\ \tilde{V}_5 \\ \vdots \end{pmatrix} = \begin{pmatrix} \Theta_1 \\ \Theta_3 \\ \Theta_5 \\ \vdots \end{pmatrix}. \quad (18)$$

The two tri-diagonal matrix systems (17) and (18) are solved by the matrix factorization method for each k. The terms of the series (10) converge as fast as $1/n$ for large n.

After solving (17) and (18), the solution is transformed back to x space by the inverse Fourier transformation

$$V_n(x) = \frac{1}{\sqrt{2\pi}} \int_{-\infty}^{\infty} \tilde{V}_n(k) e^{ikx} dk,$$

which is evaluated by Hermite integration with the 20-point formula (Abramowitz and Stegun, 1965).

Once v is known we calculate u from (3), using (4) and (5), through an expansion similar to (10), i.e.,

$$\tilde{U}_n(k) = i[-\tfrac{1}{2}\tilde{V}_{n-1} + (n+1)\tilde{V}_{n+1} - \chi(k)a_n]k^{-1}. \quad (19)$$

After having u and v we compute the geopotential ϕ from (1) to get

$$\tilde{\Phi}_n(k) = i[\epsilon\tilde{U}_n - \tfrac{1}{2}\tilde{V}_{n-1} - (n+1)\tilde{V}_{n+1}]k^{-1}. \quad (20)$$

The "vertical velocity" ω is given directly by (4).

The mean meridional circulation can be calculated by integrating (3) and (4) with respect to x:

$$\left.\begin{aligned} \frac{\partial}{\partial y}[v] &= -[X(x)]Y(y)A(p); \\ [(\ )] &\equiv \int_{-\infty}^{\infty} (\ )dx \\ [\omega] &= -[X(x)]Y(y)pS^{-1}Q(p) \\ [X(x)] &= \sqrt{2\pi} \end{aligned}\right\} . \quad (21)$$

Similarly, the east–west circulation can be obtained by integrating (3) and (4) with respect to y:

$$\left.\begin{aligned} \frac{\partial}{\partial x}\{u\} &= -X(x)\{Y(y)\}A(p); \\ \{(\ )\} &\equiv \int_{-\infty}^{\infty} (\ )dy \\ \{\omega\} &= -X(x)\{Y(y)\}pS^{-1}Q(p) \\ \{Y(y)\} &= \sqrt{2\pi}(a_0 + 2a_2 + 12a_4) \approx 0.4 \end{aligned}\right\} . \quad (22)$$

Thus, we can see that only the even terms in the expansion of $Y(y)$ in Hermite functions contribute to the east–west circulation.

b. Results of the analytical study

The meridional circulation (21) has maximum ascending motion and convergence where the heating is maximum (near the ITCZ region) and descending motion and divergence to the south in the region of cooling. Similarly, the east–west circulation (22) has its longitudinal structure given by the x-variation of the heating function $X(x)$ and depends on the net heating $\{Y(y)\}$.

Fig. 7 shows, for $\epsilon = 0.1$ (10-day dissipation time), the circulation established at low levels in response to the horizontal distribution of heating shown in Fig. 6. The geopotential and relative vorticity fields are shown in Figs. 8a and 8b, respectively.

The major result of this simple model is the establishment of a region of low pressure and cyclonic vorticity to the north and high pressure and anticyclonic vorticity to the south, but displaced westward and poleward with respect to the locations of maximum ascent and descent. Calculations with $\epsilon = 0.01$ and $\epsilon = 0.5$ show that as ϵ is decreased the low and the high move and become more elongated further westward. This is explained by the fact that in our model the slow westward moving Rossby modes, unlike the Kelvin waves, are most excited by the heating. The response becomes stationary by frictional effects, such that the smaller the dissipation the further westward the modes can travel. These results are in good agreement with some class of motions described by Gill (1980) and numerical calculations of Webster (1972). A comparison of Fig. 7 with Fig. 16b shows that this simple model is able to capture the main features of the anomalous circulation as simulated by the GCM experiment, described in the next section.

The results of this simple analytical study elucidate a possible mechanism for drought occurrence over northeast Brazil. This mechanism is essentially the establishment of a dipole type of anomalous heat source with heating to the north and cooling to the south and this can be accomplished by warm and cold SST anomalies in the tropical north and south Atlantic, respectively. The low-level anticyclonic vorticity and high pressure south of equator provides low-level divergence of moisture flux due to boundary-layer friction (not included in our simple model) and decreases rainfall over northeast Brazil.

4. A numerical experiment

We have carried out a series of numerical experiments to test the sensitivity of the GLAS general circulation model to prescribed anomalies in sea surface temperature over the tropical Atlantic. In this section we present the results of one such experiment. The results of other experiments are briefly described in the next section.

a. The GLAS climate model

The general circulation model used for this study has been described by Shukla *et al.* (1981). This is an improved version of the earlier GLAS model described by Halem *et al.* (1979). The main improvements, which have lead to a more realistic simula-

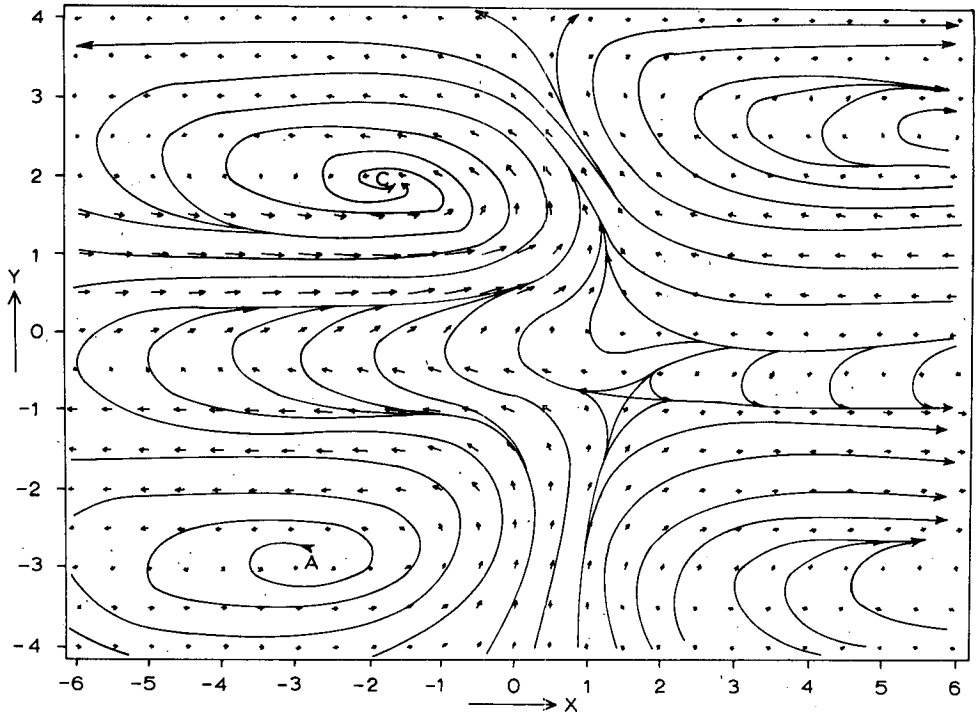

FIG. 7. Structure of analytical wind field at low levels.

tion of winter and summer circulations, are an improvement in the treatment of surface fluxes of heat and moisture and a better definition of the boundary conditions of sea surface temperature and sea ice.

It is a global model with nine sigma-coordinate levels in the vertical between the earth's surface and 65 mb, and resolves the distribution of oceans, continents and large mountain ranges reasonably well. The horizontal resolution is 4° in latitude and 5° in longitude. The longitudinal grid length along a latitude circle changes to 10° in longitude between the latitudes 66 and 78° and 20° in longitude between 82 and 90°. The climatological monthly mean sea surface temperature and sea ice is prescribed at each ocean point and changes for each calendar day. The initial snow cover and snow depth is prescribed but the model determines its own snow cover in the course of integration. The heat exchanges at the surface take place through sensible and latent heat fluxes which depend upon the surface wind, thermal stability and vertical gradients of temperature and moisture. The model contains precipitation due to supersaturation clouds and due to low, medium and deep moist convection. Rain falling through a dry layer is allowed to evaporate. The longwave radiation calculation is done every 5 h and the shortwave radiation calculation is done every 30 min. The dynamically generated clouds vary continuously in space and time and affect the shortwave and longwave radiation fluxes. The initial conditions of soil moisture are determined by the observed initial humidity near the surface and the future evolution of the soil moisture is determined by a simple ground hydrology model which accounts for the rainfall, evaporation and runoff at each land grid point.

Shukla *et al.* (1981) have examined the simulations by this model. The model simulates the global sea level pressure and global distribution of precipitation realistically. The stationary wave variance simulated by the model is much better than the earlier versions of the model and is in excellent agreement with the observed climatological stationary wave variance. The structure and magnitudes of the simulated cyclone-scale variance also is very well simulated. The low-frequency planetary waves are not well simulated. The simulated variances and covariances of momentum, heat and moisture have been compared only with the climatological observations for the Northern Hemisphere because a reliable climatology of variances and covariances and their interannual variability has not yet been compiled for the Southern Hemisphere. The simulation of the mean fields for the Southern Hemisphere is also quite reasonable. It should be pointed out, however, that an underlying assumption in carrying out the sensitivity experiments with general circulation models is that, although the model may not be perfect in reproducing the mean climate, it could provide realistic estimates of the perturbations in the mean climate in response to a

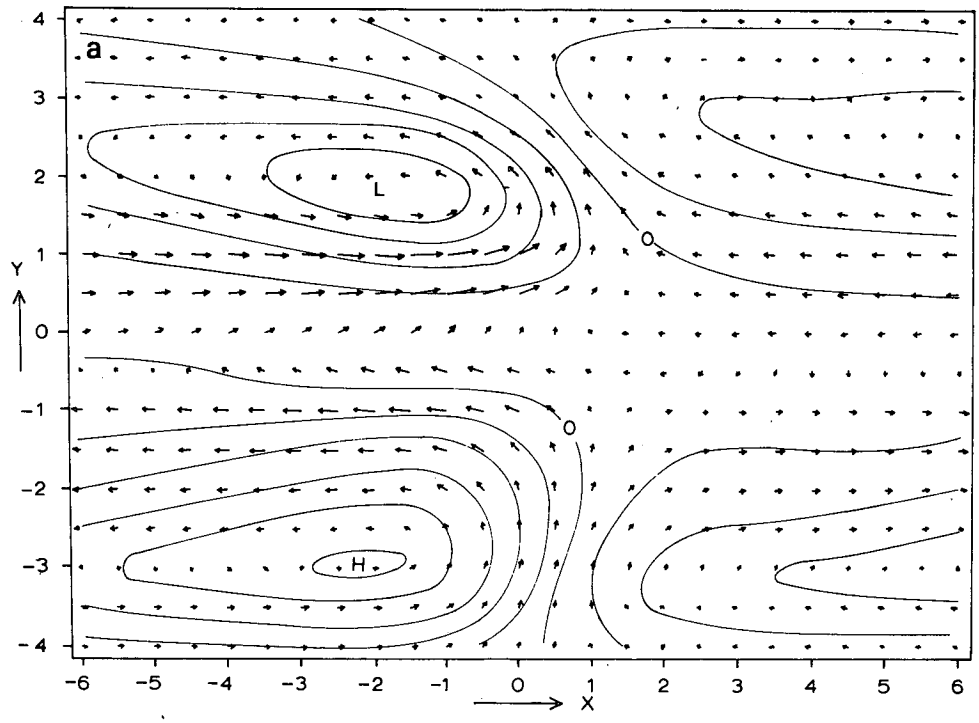

FIG. 8a. Structure of the geopotential field superimposed on the wind field.

prescribed external forcing. For example, the mean precipitation over northeast Brazil in the mean simulation is larger than the observed precipitation. This could have been due to low values of surface albedo over the Northeast prescribed for the mean simulation. This does not invalidate the model to test its sensitivity to prescribed changes in sea surface temperature because the simulations with SST

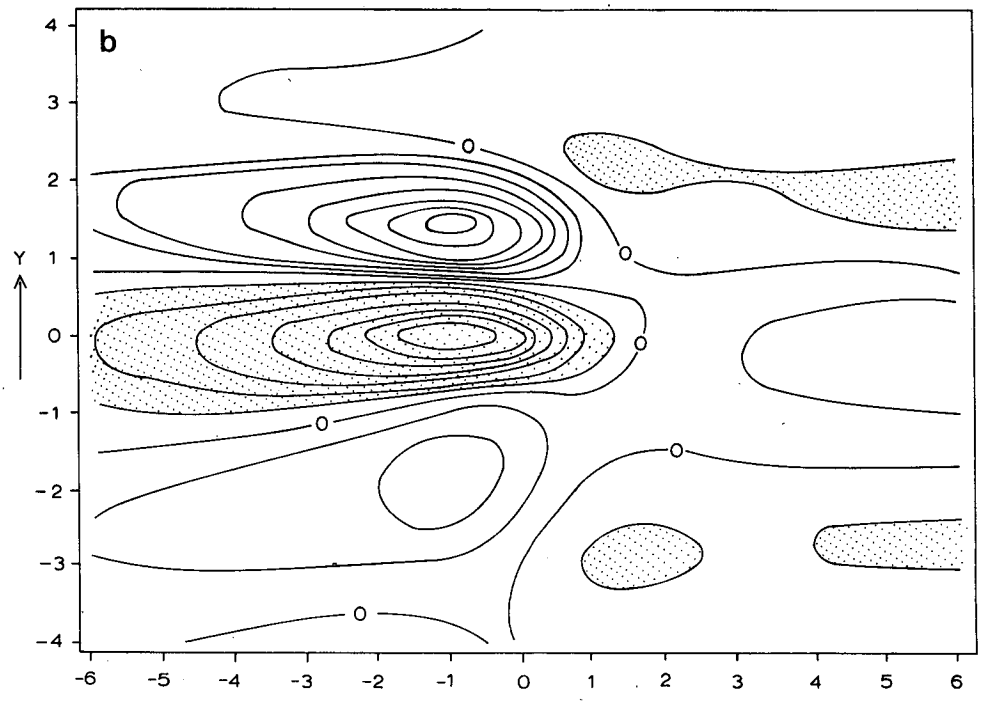

FIG. 8b. Structure of analytical vorticity field corresponding to Fig. 7. Negative values are shaded.

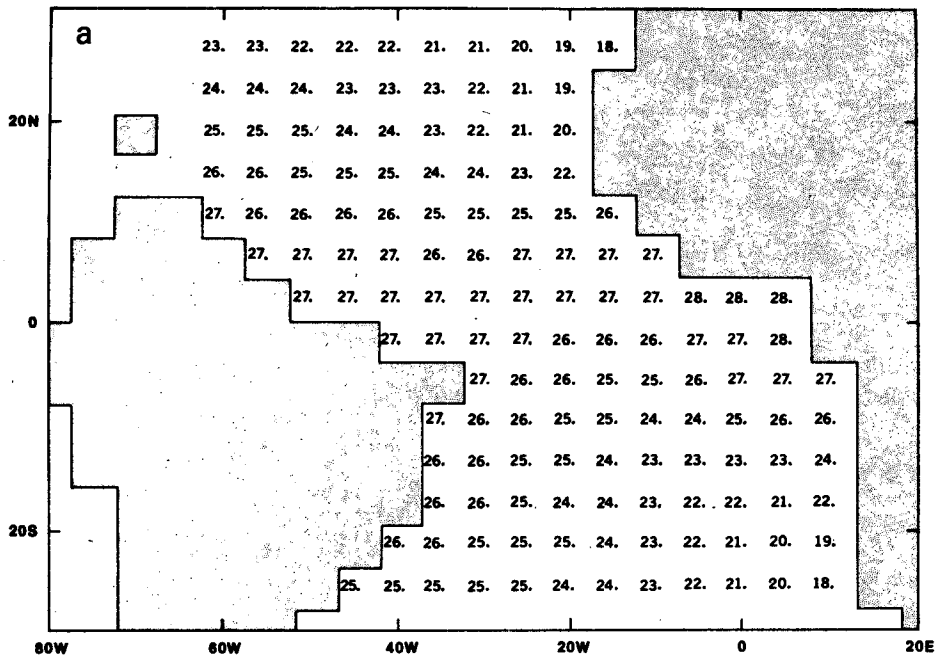

FIG. 9a. Sea surface temperature (°C) for January used in the control run.

anomaly will also contain the same albedos and other boundary conditions as the mean simulation.

b. The experiment

The model was first integrated for 90 days with climatological sea surface temperature. The mean January sea surface temperature over the Atlantic is shown in Fig. 9a. The initial conditions were taken from the observations of 1 January 1975. Then the SST anomaly shown in Fig. 9b was superimposed over the climatological sea surface temperature and the SST anomaly was assumed to be constant for 90 days. Starting from the atmospheric

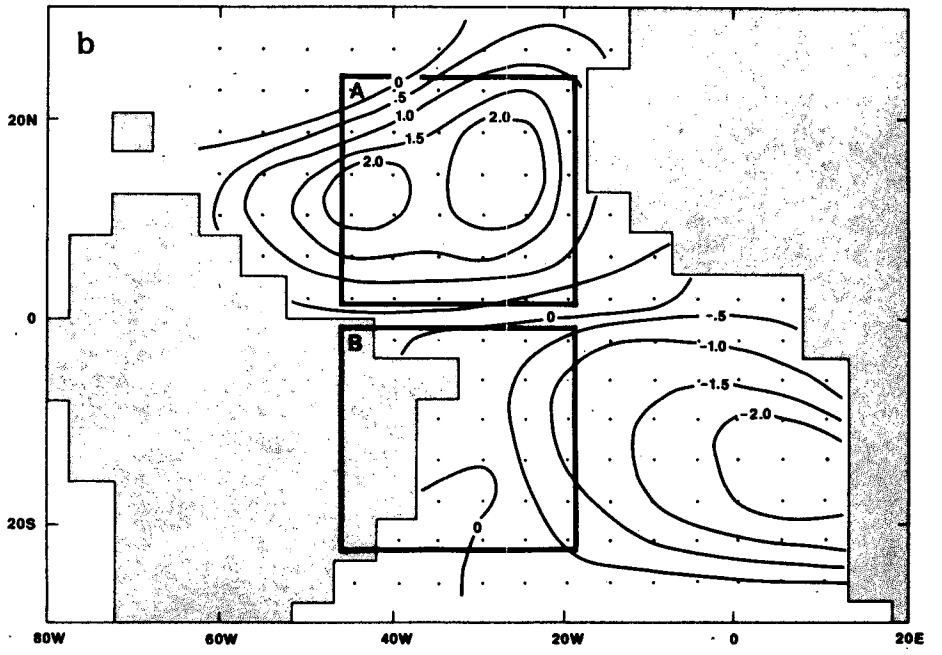

FIG. 9b. Sea-surface temperature anomaly (°C) for the anomaly run. Thick lines enclose area A (upper) and area B (lower).

initial conditions identical to the first run, the model was integrated again for 90 days. We will refer to these two integrations as the control run and the anomaly run, respectively. It was found that after 60 days the differences between the two runs, especially in the polar regions, were very large. We have not yet investigated the structure and mechanism of the response after 60 days. In the present paper we have analyzed the results of first 60 days which is considered an adequate length of integration to test the sensitivity of tropical SST anomalies.

It would have been more appropriate to integrate the model equations starting from the initial conditions of March. However, since we were mainly interested in the differences between the control run and the anomaly run, the present model runs were considered to be adequate to give the model response of the prescribed SST anomalies. It is reasonable to assume that after the first 30 days of integration the model forgets the initial conditions almost completely. Moreover, a 90-day integration (control run) was already available to us and we had to make only the anomaly run for 90 days.

c. *Sea surface temperature anomaly*

Sea surface temperature anomalies in low latitudes are considered to be one of the important forcings for interannual variability of monthly means (Charney and Shukla, 1981). Due to a highly nonlinear relation between temperature and saturation vapor pressure, small SST anomalies change evaporation and moist convection substantially. The anomalous thermal wind also is relatively larger in the tropics. Earlier numerical experiments have shown significant response of monsoon circulation to SST anomalies over the Arabian Sea (Shukla, 1975) and large local and midlatitude response to SST anomalies in other parts of tropics (Rowntree, 1976; Julian and Chervin, 1978).

In the present study we have examined the response of the GLAS model to SST anomalies over the tropical Atlantic. The SST anomaly pattern was chosen to correspond to that given by Hastenrath and Heller (1977) for drought over northeast Brazil. Fig. 9b shows the SST anomaly used for the numerical experiment. The magnitudes of the anomalies were chosen to be comparable to the maximum values observed during the 25-year period. Thus, the SST anomalies used in this experiment are larger than actual observed anomaly in any year, but not larger than 0.5–1.0°C.

d. *Results of numerical experiments*

We have examined the time-averaged and transient characteristics of the response due to the prescribed SST anomaly. We present below the differences between the anomaly run and the control run for sea level pressure, geopotential height, rainfall, wind field, evaporation, vertically integrated moisture flux convergence and meridional circulation. We have looked into the global structure of the response and we present only those global fields which were found to be relevant for our analysis and interpretation. Therefore, we have mainly presented and emphasized the structure of the response in a limited region in the neighborhood of the tropical Atlantic.

c. *Rainfall*

Fig. 10 shows the 15-day running mean time series of daily rainfall averaged over the areas A and B (shown in Fig. 9) for control and anomaly runs. Although the spatial resolution is not adequate to resolve small-scale phenomena, the natural variability of the model shows spatially inhomogeneous structure and, it is therefore necessary to average the daily rainfall over sufficiently large areas. Area B contains the northeast Brazil region and the neighboring oceans with a cold SST anomaly. Area A includes the region of warm SST anomaly. The rainfall over area A increases due to the warm SST anomaly and a shift of the ITCZ from area B in the control run to area A in the anomaly run. In the anomaly run the mean rainfall in area A remains larger than the control run for all 90 days. The rainfall in the control and anomaly runs is comparable for the first 10 days but for days 20–60, the anomaly run has less rainfall than the control run. Although the 60- or 90-day mean rainfall for area B is smaller for the anomaly run compared to the control run, the difference is not systematic after 60 days. Internal model adjustments make the two rainfall series indistinguishable during days 60–90. We have not examined as to how the internal dynamics affected by the SST anomaly in turn affects the rainfall over the regions of our interest. The results clearly show, however, that for first 60 days the rainfall decreases to the south and increase to the north. Sixty-day integrations are considered adequate to detect the influence of tropical SST anomalies (Washington and Chervin 1979).

We also examined the daily time series of other dynamical fields to explain the large fluctuations in rainfall between days 60 and 90. Fig. 11 shows the daily time series of zonally averaged sea level pressure differences between the control run and the anomaly run. The differences exceed 30 mb in the north polar regions and 15 mb in the south polar regions. A similar calculation for differences between longitudes 60°W and 10°E show similar large values over larger parts of the polar regions. These, being just the average of differences and not the root-mean-square (rms) differences, are very large and suggest a possible manifestation of the global-scale response. In the present study we have not investi-

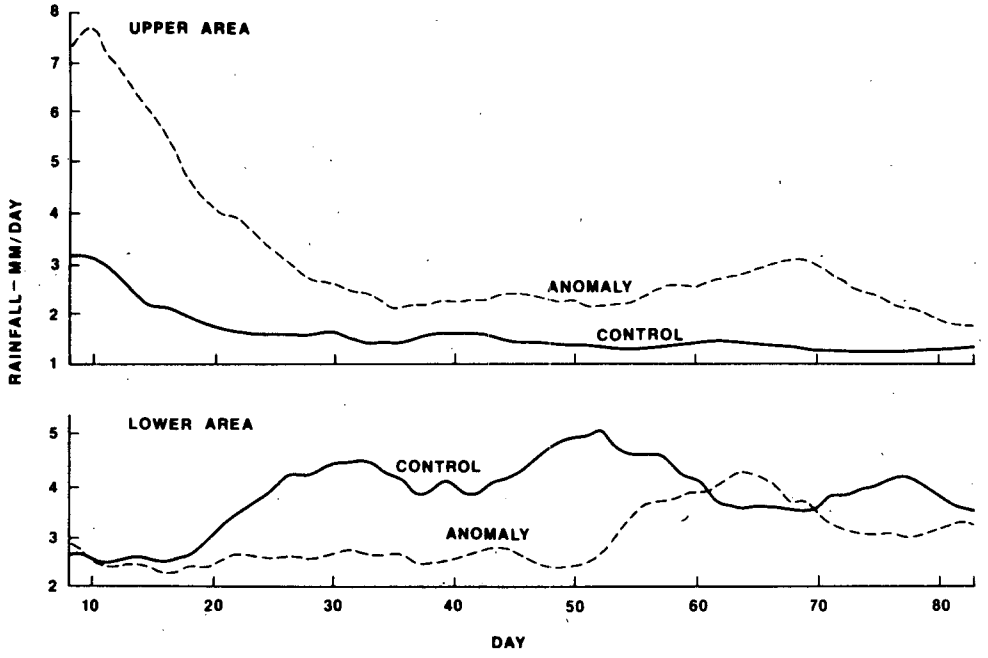

FIG. 10. 15-day running mean of daily rainfall (mm day^{-1}) for upper (area A) and lower (area B) areas.

gated the structure of the dynamical response after 60 days and we have confined our analysis to the time averages for the first 60 days only. For calculating the lag-correlation functions of daily rainfall, we have used the complete 90-day time series.

Following Leith (1973) and Shukla (1975), we calculated the values of σ_T^2, a measure of error in estimating the time mean for period T (=30 days):

$$\sigma_T^2 = \frac{2\sigma^2}{T}\int_0^T \left(1 - \frac{\tau}{T}\right)R(\tau)d\tau.$$

Here σ^2 is the standard deviation of daily rainfall values. For calculating the lag-correlation function $R(\tau)$, we use the positive definite estimate of covariance function.

$$R(\tau) = [N^{-1}\sum_{t=1}^{N}\{x(t+\tau) - \bar{x}\}\{x(t) - \bar{x}\}] \times [N^{-1}\sum_{t=1}^{N}\{x(t) - \bar{x}\}^2]^{-1},$$

where x is daily rainfall and $N = 90$.

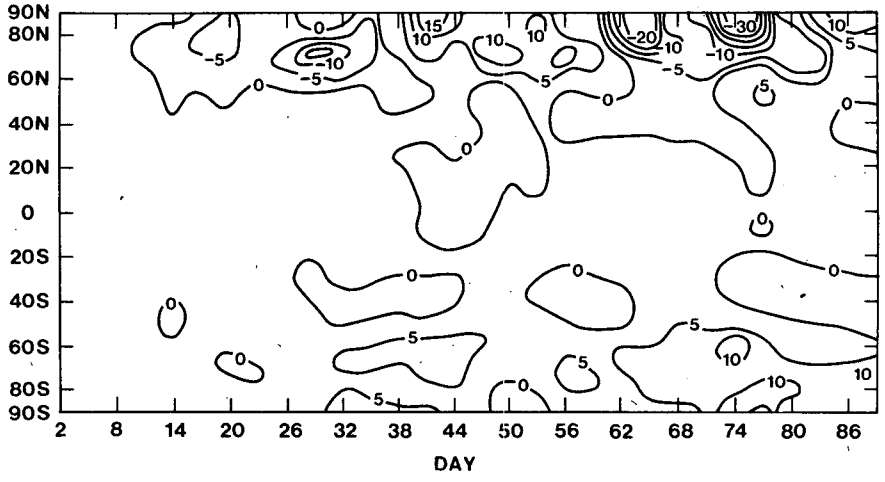

FIG. 11. Latitude-time cross section of differences between zonally averaged sea level pressure (mb) for anomaly and control runs.

We first detrended the 90-day time series of daily rainfall over areas A and B by fitting a parabola. The value of σ_T for 30-day mean rainfall over warm SST (area A) and cold SST (area B) were found to be 0.13 and 0.16 mm day^{-1}, respectively. Such small values of σ_T are due to negative values of the autocorrelation function. For area A the ratio $(\Delta\mu/\sigma_T)$, (where $\Delta\mu$ is the difference of mean rainfall for the anomaly and control runs) was found to be 6 and 7 for 30-day (day 31–60) and 60-day (day 31–90) mean rainfall, and -10 and -5 for similar 30- and 60-day mean rainfall over area B. If instead of a parabola, only the 90-day mean was removed from the time series, the values of σ_T for areas A and B were 0.45 and 0.49 mm day^{-1}, respectively. The ratio $(\Delta\mu/\sigma_T)$ was 1.7 and 2.1 for 30- and 60-day mean rainfall over area A, and 3.3 and 1.8 for area B. In either case the ratio is found to be larger than unity.

Fig. 12a shows the ratio of 60-day mean differences between the anomaly and control runs, and standard deviations among 60-day means for nine runs with an earlier version of the model (Halem *et al.*, 1979) with identical boundary conditions. Ideally, we would have preferred to integrate the present model for several years to determine the natural variability of the model for climatologically prescribed sea surface temperatures; however, due to limitations of computing resources we could not carry out such long integrations. The internal dynamics of the model can produce seemingly large differences even in the absence of prescribed forcings due to SST anomalies and it requires rigorous, but not necessarily illuminating, statistical significance tests to determine the significance level of the result. Here we are not searching for a possible response but we have used the general circulation model to verify the validity of a mechanism suggested by analysis of observations and results of a simple analytical model.

The maximum values of the ratio are found to occur over the region of ITCZ displacement. Since the ITCZ is displaced northward, the maximum positive departures occur over the regions of the ITCZ in the anomaly run and maximum negative departures occur in the region of the ITCZ in the control run. In the following analysis we have examined a limited region only. There is also found to be a large ratio for south tropical Pacific and other smaller regions for which we have not studied the physical reality of the response.

Fig. 12b shows the 60-day mean rainfall differences between the anomaly and the control runs.

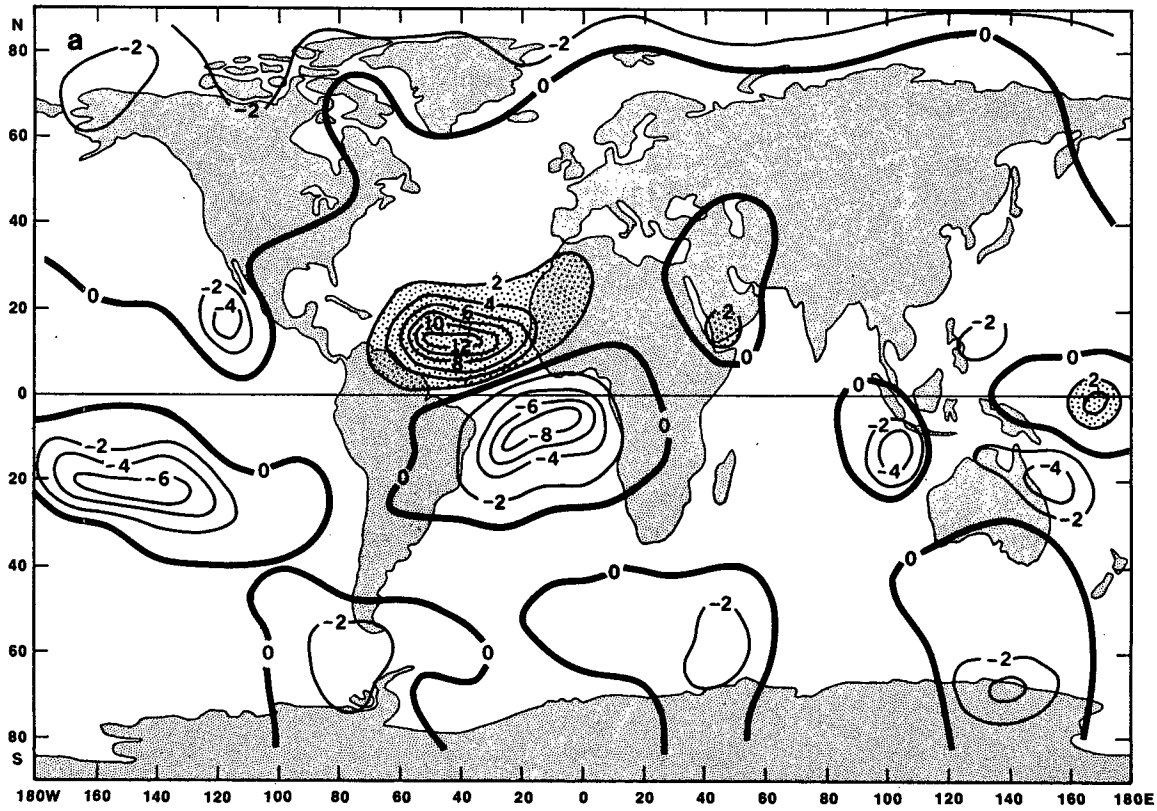

FIG. 12a. Ratio of 60-day mean rainfall difference (anomaly-control) and standard deviation among 60 day mean rainfall for nine control simulations.

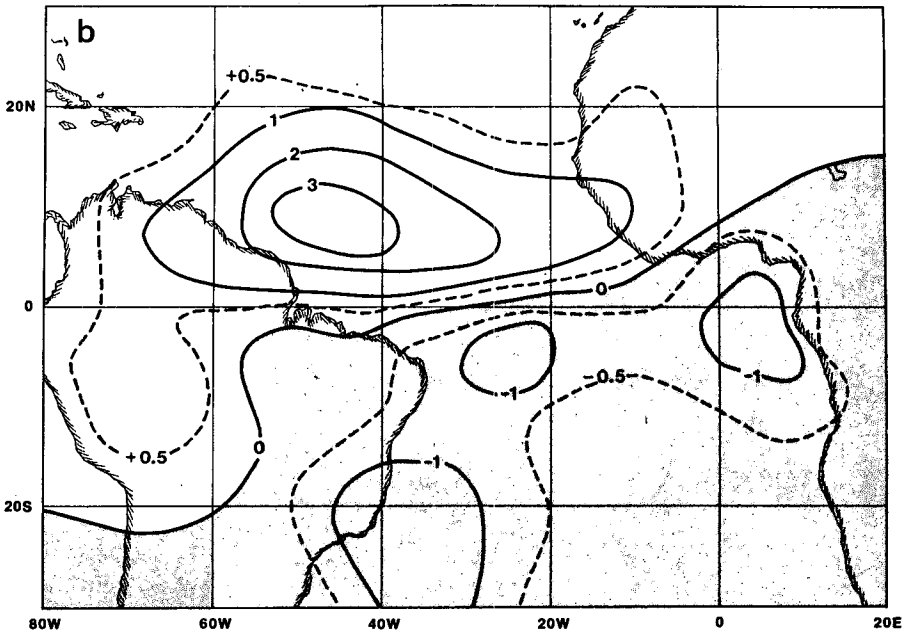

FIG. 12b. Difference (anomaly-control) of 60-day mean rainfall (mm day^{-1}).

The differences were smoothed by a 5-point smoother except along 2°N and 2°S where no averaging was done across the latitudes. There is a clear increase in the rainfall over warm SST anomalies to the north and a decrease in the rainfall over cold SST anomalies to the south. Most of the northeast Brazil region shows a decrease in the rainfall. Although the maximum reduction of the rainfall occurs over the oceans adjacent to northeast Brazil, the differences over the land are large enough to support the basic proposed mechanism. Although there is not sufficient observed rainfall data over the oceans to document this phenomenon, it is our conclusion, based on these numerical and analytical results, that the drought over the Northeast occurs in association with a reduction in the rainfall over a larger region adjacent to northeast Brazil. An increase in the rainfall over northern South America, in association with droughts over the Northeast, is found to be consistent with the observational findings of Hastenrath and Heller

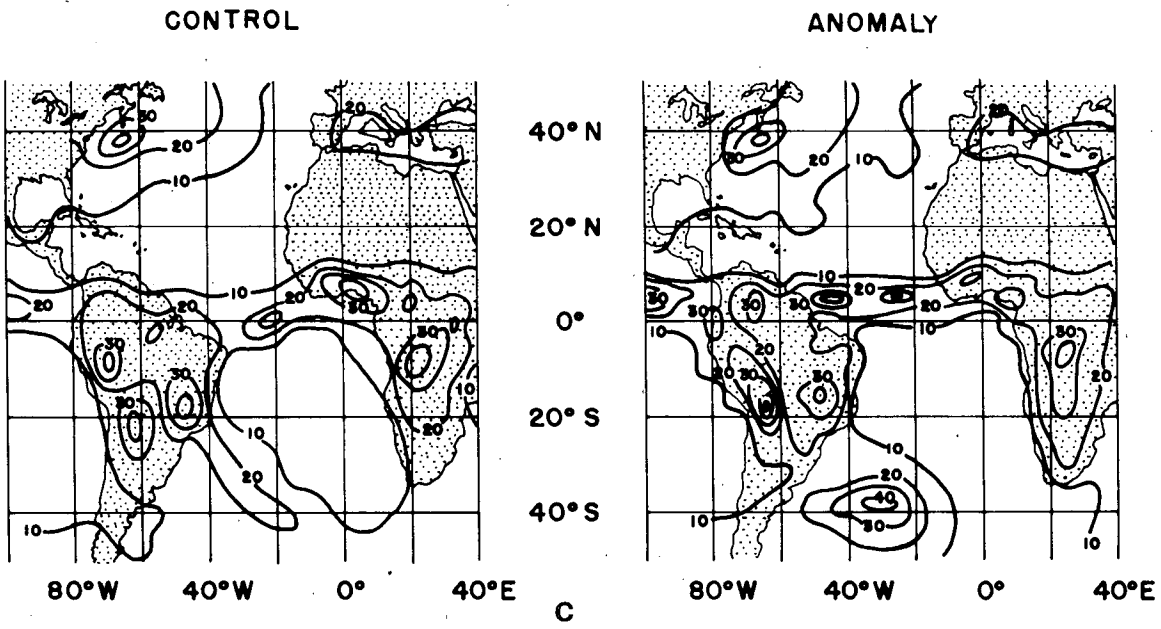

FIG. 12c. Monthly mean rainfall (10^{-2} mm h^{-1}) for control and anomaly run.

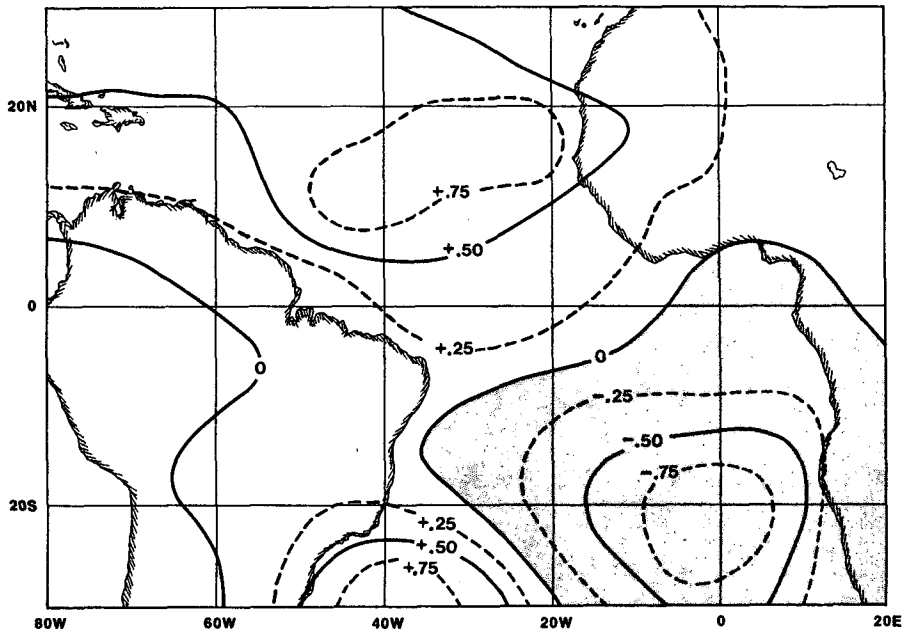

FIG. 13. Differences (anomaly-control) of 60-day mean evaporation.

(1977). The northward displacement of the ITCZ is seen more clearly in Fig. 12c.

f. Evaporation and vertically integrated moisture flux convergence

We have attempted to clarify the mechanism of the rainfall reduction over the Northeast by examining the moisture budget over the whole region. Figs. 13 and 14 give the 60-day mean differences for evaporation and vertically integrated moisture flux convergence, respectively. The reduction in the evaporation over the ocean adjacent to the Northeast is negligibly small. The largest reductions (0.5–0.75 mm day^{-1}) in evaporation occur around 20°S, 5°W and similar increases in evaporation occur around 15°N, 40°W. These areas coincide with the areas of coldest and warmest SST anomalies. The

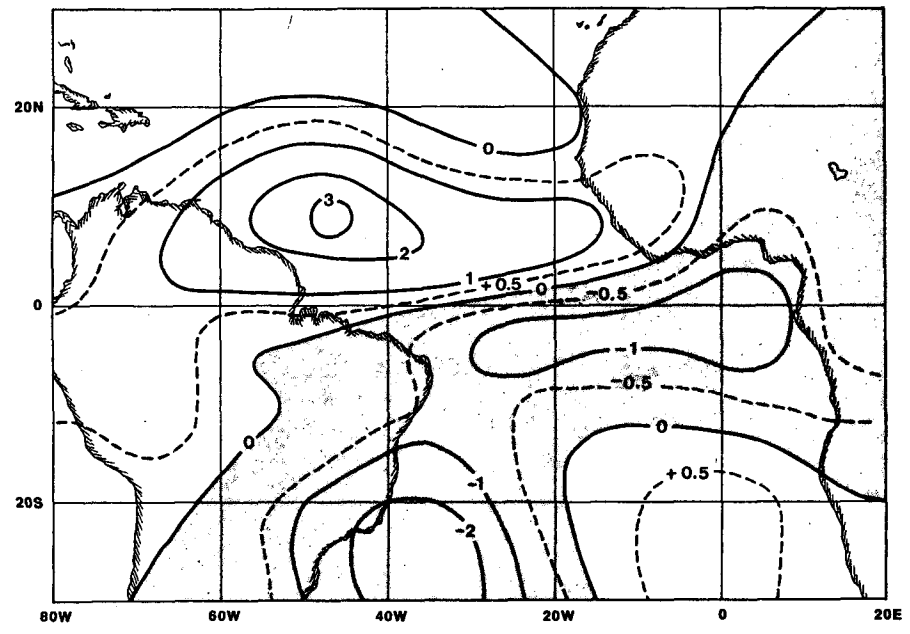

FIG. 14. Differences (anomaly-control) of 60-day mean vertically integrated moisture flux convergence.

reduction in the rainfall over the coldest anomalies is not as large as the reduction in evaporation because, due to changes in circulation, a northward shift of subtropical high is nearly compensated by an increase in the vertically integrated moisture flux convergence. An apparent similarity in the patterns of vertically integrated moisture flux convergence differences and rainfall differences suggests that most of the reduction in rainfall over northeast Brazil and adjoining oceans is dynamically controlled. A northward shift of the ITCZ and descending motion to the south of equator causes a decrease in the moisture flux convergence and reduction in the rainfall. The maximum increase in the vertically integrated moisture flux convergence along 10°N is associated with low-level convergence over the warm SST anomaly and a northward shift of the North Atlantic subtropical anticyclone, which also gives rise to reduced moisture flux convergence further north.

g. Meridional circulation

Fig. 15 shows the differences of the first 60-day mean meridional circulation averaged between 50°W and 5°E. The anomalous meridional circulation shows an ascending branch with maximum vertical motions between 5 and 10°N and a descending branch to the south of the equator. It is this descending motion over the northeast Brazil region which is one of the most important factors in producing the drought. We have not explained here why a SST anomaly over the North Atlantic produces a meridional circulation whose scale is ~2000 km; however, it is comparable to the Rossby radius of deformation for equatorial motions. Descending motion to the south of the equator reduces the vertically integrated moisture flux convergence, which, coupled with reduction in evaporation over the ocean, reduces rainfall in the Northeast.

h. Circulation at 850 mb

Fig. 16a shows the monthly mean wind vectors for days 16–45 at 850 mb for the control and anomaly runs. In the control run the center of the North Atlantic subtropical anticyclone is at about 20°N, whereas in the anomaly run it is further north. The northerly flow to the east of the center is more organized and stronger. Similarly, the South Atlantic subtropical anticyclone also has moved northward. The anomalous vorticity and divergence fields (not shown) also were examined and it was found that vorticity increased to the north and divergence increased to the south of the equator. These results are consistent with the observational findings of Hastenrath and Heller (1977) who found that the composite circulations for drought years were "characterized by an equatorward expansion of the South Atlantic and a poleward retraction of the North Atlantic high." Fig. 16b shows the difference between the wind vectors for the anomaly and con-

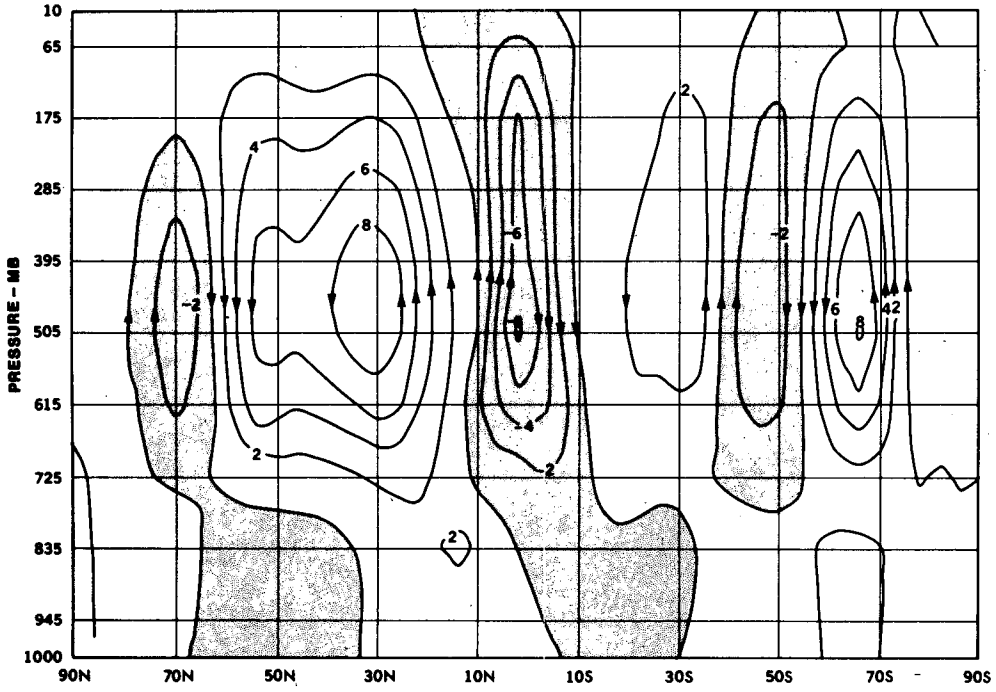

FIG. 15. Difference of 60-day mean meridional circulation (10^{13} g s^{-1}) averaged between the longitudes 50 and 5°W.

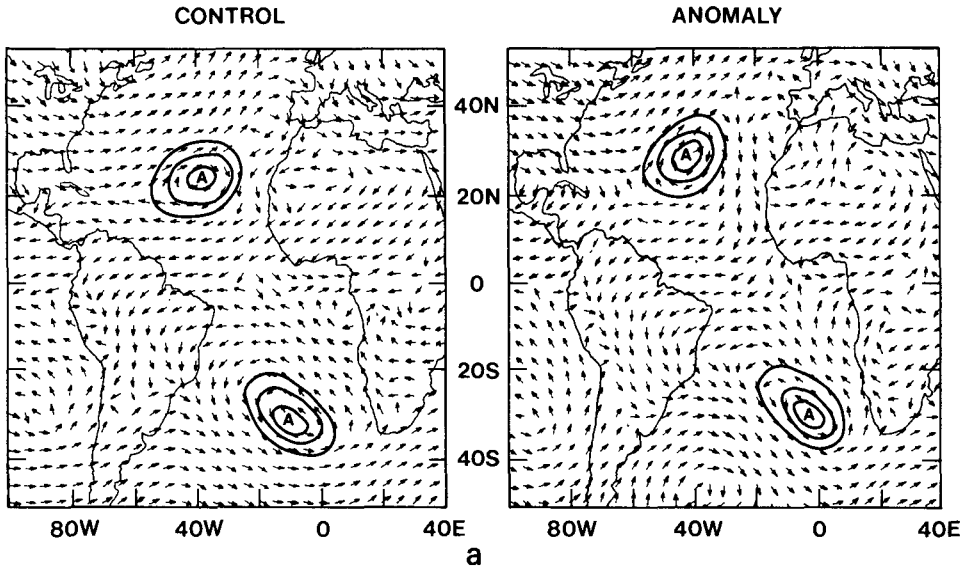

FIG. 16a. Monthly mean wind vectors for control and anomaly run at 850 mb.

trol runs at 700 mb. An anomalous cyclonic circulation is found to the north and anticyclonic circulation to the south.

In agreement with the earlier conclusions of Charney and Shukla (1981), this study suggests that the SST anomalies in low latitudes can change the large-scale Hadley- and Walker-type circulations which are otherwise stable with respect to dynamic instabilities. It can be speculated that the interannual variability of the location and intensity of the subtropical highs may be related to the variability of the tropical heat sources.

i. Sea level pressures

Fig. 17 shows the differences for the 60-day mean sea level pressure between the anomaly and control runs. A constant value of 1.23 mb was subtracted at each grid point to show the gradients of the anomaly field. As expected, hydrostatic negative departures

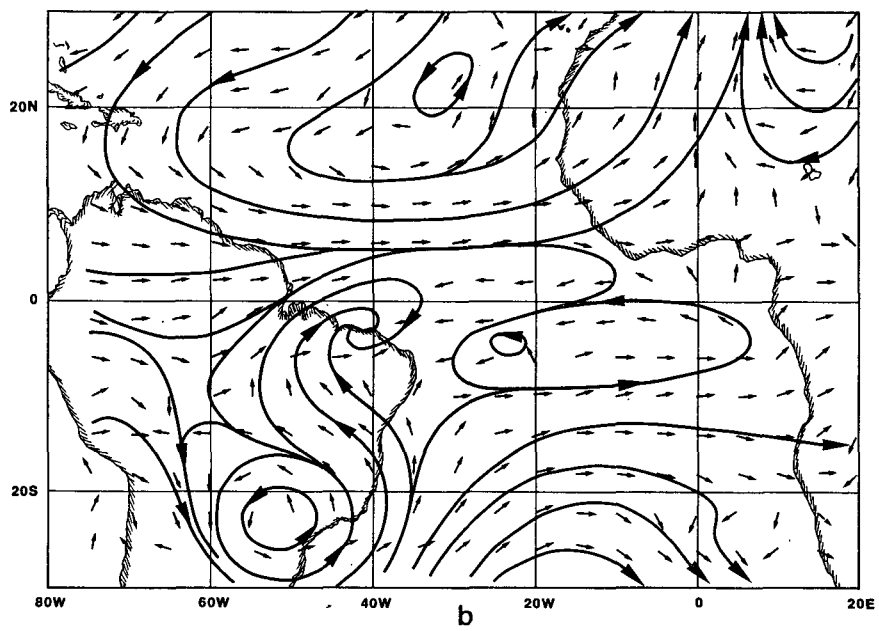

FIG. 16b. Differences (anomaly-control) of 60-day mean wind vectors at 700 mb.

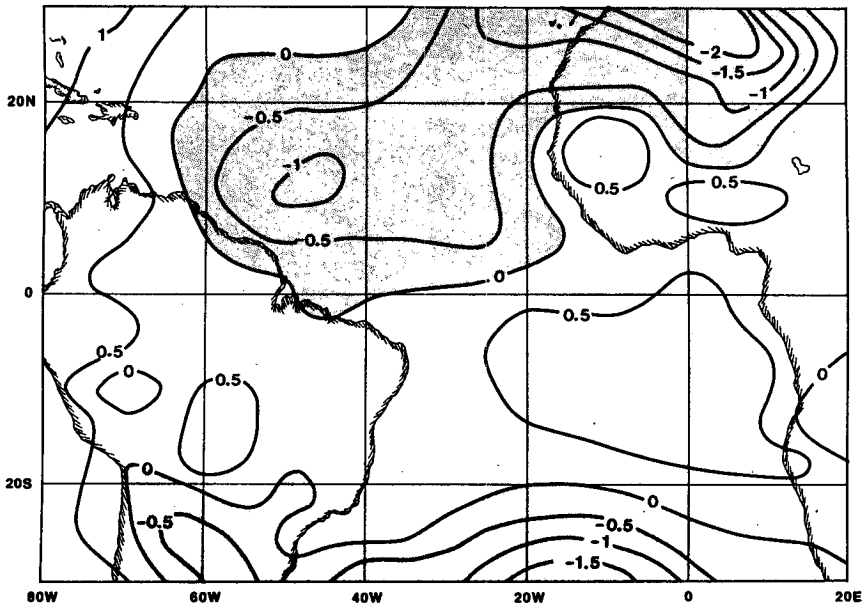

FIG. 17. Differences (anomaly-control) of 60-day mean sea level pressure (mb.).

occur in association with warm SST anomalies to the north of the equator and positive departures occur to the south of equator. This is in qualitative agreement with the composite patterns for drought years shown by Hastenrath and Heller (1977), although their observed sea level pressure anomalies are not spatially homogeneous. Examination of daily model-generated sea level pressure anomalies revealed that large fluctuations occur due to large-scale pressure oscillations associated with extratropical disturbances.

j. Geopotential height

Fig. 18 shows the differences between the anomaly and control runs for 30-day mean geopotential heights at 850 mb. The difference field has similar structure at 500 and 300 mb suggesting the barotropic nature of the response. Although the natural variability of monthly means during the Northern Hemisphere winter is usually larger at middle latitudes, the observed changes are larger than the natural variability of the model. These results seem to confirm the suggestions by Namias (1972) and Meehl and van Loon (1979) that extratropical general circulation in the Atlantic may be related to tropical variability. The present study suggests that the tropical heat sources are the primary driving mechanisms for the observed teleconnections.

5. Conclusions

Observational analysis of 25 years of SST anomalies over the tropical Atlantic and rainfall over selected stations in northeast Brazil suggests that simultaneous occurrences of warm SST anomalies to the north and cold SST anomalies to the south of the equator are related to droughts over the Northeast. This is in agreement with earlier observational studies of Markham and McLain (1977) who examined the SST anomalies only to the south of the equator, and Hastenrath and Heller (1977) who prepared the composite maps for drought years. A simple analytical model with prescribed heating and cooling to the north and south of the equator, respectively, shows that meridional circulations forced by such a thermal forcing cause descending motion and anticyclonic vorticity to the south and ascending motion and cyclonic vorticity to the north.

These results have lead us to suggest that a possible mechanism for drought over northeast Brazil is the intensification of the ITCZ to the north of the equator, which occurs in association with warm SST anomalies, and establishment of descending motion over northeast Brazil and adjoining oceans with cold SST anomalies, which reduces moist convection and rainfall. The simultaneous occurrence of warm SST anomalies in the north and cold SST anomalies in the south reinforces this mechanism. We have not examined the stability of the ITCZ with respect to symmetric displacements; however, based on numerical experiments with a global general circulation model, we conclude that sufficiently warm SST anomalies (1–2°C), especially in the western sector of tropical North Atlantic, where the mean sea surface temperature is relatively high, tend to anchor the ITCZ to the north and reduce rainfall in the Northeast.

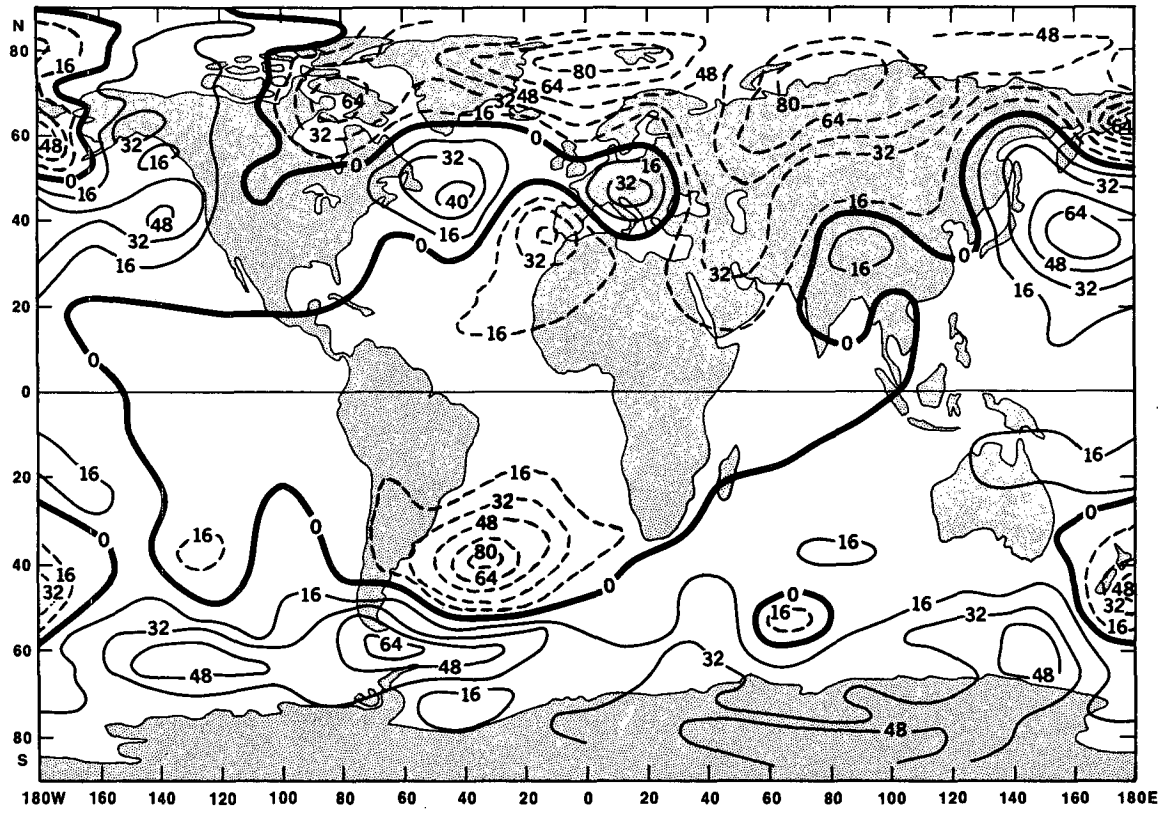

FIG. 18. Differences (anomaly-control) of 30-day mean geopotential height (gpm) at 850 mb.

We have carried out a series of numerical experiments to test the sensitivity of the GLAS general circulation model to the prescribed SST anomalies over the tropical Atlantic. When the prescribed SST anomaly is similar to the composite patterns for drought years given by Hastenrath and Heller (1977), the model shows a reduction in the rainfall over northeast Brazil. In two separate experiments (not described here), it was found that a warm SST anomaly over the western sector of the tropical North Atlantic is much more effective than a warm SST anomaly near the African coast. We have not carried out the required numerical experiments to determine the relative importance of warm SST anomalies in the north and cold SST anomalies in the south.

The results of the numerical experiments further support the validity of the proposed mechanism. Warm SST anomalies in the north and cold SST anomalies in the south cause intensification and northward displacement of the ITCZ. The vertically integrated moisture flux increases to the north and decreases to the south. The role of reduced evaporation in the south and increased evaporation in the north seems to be secondary for moisture balance. The dynamical circulation forced by the diabatic heat source in the north seems to be the most important determinant of the fluctuations of rainfall over northeast Brazil. In the anomaly experiments, the North and South Atlantic subtropical anticyclones are displaced northward which is consistent with northward displacement of the ITCZ and is in agreement with the observations of Hastenrath and Heller (1977) for drought years. The experiments also show an increase in the rainfall over northern South America in association with a decrease in the rainfall over the Northeast. This is also in agreement with the observational evidence. While examining the global response of the prescribed SST anomalies we have also noticed tropical–extratropical teleconnections consistent with the observations of Namias (1972) and Meehl and van Loon (1979), and the model calculations of Hoskins *et al.* (1977). We speculate that tropical heat sources are the primary mechanisms for these teleconnections.

We have not investigated the mechanisms which produce these SST anomalies over the Atlantic. However, these anomalies are found to persist for several months and, therefore, they are potential tools for predicting droughts in northeast Brazil.

Acknowledgments. This study is an outcome of a collaborative effort between the Institute for Space

Research (CNPq/INPE), Brazil and the National Aeronautics and Space Administration (NASA), USA. We would like to thank these organizations for their support and encouragements. We are thankful to Dr. Milton Halem for his support and encouragement to conduct this study at the GLAS Modeling and Simulation Facility. We have greatly profited from several stimulating discussions with Professor Jule G. Charney and Mr. Carlos Nobre. We thank Dr. Jack Calman for providing maps of SST anomalies and Messrs. W. T. Johnson, T. Upton, R. Sabatino, and L. Marx for their help in conducting the GCM experiments. We are grateful to Dr. K. C. Mo who helped with the numerical calculations in the analytical study. We also thank Miss Karen DeHenzel and Miss Debbie Boyer for efficiently typing the manuscript.

One of the authors (A.D.M.) would like to thank Drs. Nelson Jesus Parada and Luiz Gylvan Meira Filho for their encouragement and interest in this work and Drs. Luiz Baldicero Molion and Vernon E. Kousky and Mr. Julio Buchmann for many helpful discussions on the northeast Brazil climate. This research was partially financed by Convenio FINEP/CNPq B28/79/002 Modelagem Atmosferica and PTSA/CNPq-Polo Nordeste 37/78.

REFERENCES

Abramowitz, M., and I. A. Stegun, 1965: *Handbook* of *Mathematical Functions*. Dover, 1046 pp.

Aldaz, L., 1971: A partial characterization of the rainfall regime of Brazil. DNMET, Vol. 1 (SUDENE, Publicacao Tecnica, 4), Rio de Janeiro.[2]

Bjerknes, J., 1969: Atmospheric teleconnections from the equatorial Pacific. *Mon. Wea. Rev.*, **97**, 163–172.

Bunker, A., 1976: Computations of surface energy flux and annual air-sea interaction cycles of the North Atlantic ocean. *Mon. Wea. Rev.*, **104**, 1122–1140.

Carvalho, J. O., 1973: Uma avaliacao dos metodos de previsao de secas para o Nordeste do Brasil. *Plano Integrado para o Combate Preventivo aos Efeitos das Secas no Nordeste*. J. O. Carvalho, Ed. (An evaluation of drought forecasting methods for Northeast Brazil), Ministerio do Interior, Serie Desenvolvimento Regional, 1, 193–220. [Available from SUDENE, Recife, PE; Brazil].

Caviedes, C. N., 1973: Secas and El Niño: Two simultaneous climatical hazards in South America. *Proc. Assoc. Amer. Geograph.*, **5**, 44–49.

Charney, J. G., 1975: Dynamics of desert and drought in the Sahel. *Quart. J. Roy. Meteor. Soc.*, **101**, 193–202.

——, and J. Shukla, 1981: Predictability of monsoons. *Monsoon Dynamics*, Sir James Lighthill and R. P. Pearce, Eds., Cambridge University Press, 99–109.

Covey, D. L., and S. Hastenrath, 1978: The Pacific El Niño phenomenon and the Atlantic circulation. *Mon. Wea. Rev.*, **106**, 1280–1287.

Cunha, Euclides da, 1940: *Os Sertoes* (Campanha de Canudos). (The Hinterlands). Francisco Alves, Rio de Janeiro, 646 pp.

Derby, O. A., 1885: As manchas solares e as seccas (The sun spots and the droughts). Revista de Engenharia, **8**, 112–114.

Gill, A. E., 1980: Some simple solutions for heat-induced tropical circulation. *Quart. J. Roy. Meteor. Soc.*, **106**, 447–462.

Gomes Filho, M. F., 1979: Um estudo sobre a influencia do albedo diferencial e da orografia na circulacao atmosferica: Uma aplicacao'para o Nordeste brasileiro (A study of differential albedo and orographical influence on the atmospheric circulation: Application to Northeast Brazil). M. Sc. thesis, INPE-1640-TDL/015, 86 pp. [Available from INPE-C.P. 515, 12.200 Sao Jose dos Campos, S.P., Brazil.]

Halem, M., J. Shukla, Y. Mintz, M. L. Wu, R. Godbole and Y. Sud, 1979: Climate comparisons of a winter and summer numerical simulation with the GLAS general circulation model. *GARP Publ. Ser.*, **22**, 207–253.

Hastenrath, S., 1978: On modes of tropical circulation and climate anomalies. *J. Atmos. Sci.*, **35**, 2222–2231.

——, and L. Heller, 1977: Dynamics of climate hazards in Northeast Brazil. *Quart. J. Roy. Meteor. Soc.*, **103**, 77–92.

——, and P. J. Lamb, 1977: *Climatic Atlas of the Tropical Atlantic and Eastern Pacific*. University of Wisconsin Press, 109 pp.

Henry, A. J., 1922: The rainfall of Brazil. *Mon. Wea. Rev.*, **50**, 412–417.

Hoskins, B. J., A. J. Simmons and D. G. Andrews, 1977: Energy dispersion in a barotropic atmosphere. *Quart. J. Roy. Meteor. Soc.*, **103**, 553–567.

Hull, F. R., 1942: A frequencia das secas no Estado do Ceara e sua relacao com a frequencia dos anos de manchas solares minimas (The frequency of droughts in Ceara state and its relationship with the frequency of years with sun spot mimima). Boletim da Secretaria da Agricultura e Obras Publicas, **4**, 58–63.

Jones, R. H., and J. P. Kearns, 1976: Fortaleza, Ceara, Brazil rainfall. *J. Appl. Meteor.*, **15**, 307–308.

Julian, P. R., and R. M. Chervin, 1978: A study of the Southern Oscillation and Walker Circulation phenomenon. *Mon. Wea. Rev.*, **106**, 1433–1451.

Kousky, V. E., 1979: Frontal influences on Northeast Brazil. *Mon. Wea. Rev.*, **107**, 1140–1153.

——, 1980: Diurnal rainfall variation in northeast Brazil. *Mon. Wea. Rev.*, **108**, 488–498.

——, and P. S. Chu, 1978: Fluctuations in annual rainfall for northeast Brazil. *J. Meteor. Soc. Japan*, **57**, 457–465.

Leith, C., 1973: The standard error of time-average estimates of climatic means. *J. Appl. Meteor.*, **12**, 1066–1069.

Lindzen, R. D., 1967: Planetary waves on beta-planes. *Mon. Wea. Rev.*, **95**, 441–451.

Marinho, M. E., and A. C. Reboucas, 1971: Hidrologia das Secas–Nordeste do Brasil (Hydrology of droughts—Northeast Brazil). Superintendencia de Desenvolvimento do Nordeste (SUDENE), Recife. [Available from SUDENE, Recife, PE; Brazil].

Markham, C. G., 1974: Apparent periodicities in rainfall at Fortaleza, Ceara, Brazil. *J. Appl. Meteor.*, **13**, 176–179.

——, and D. R. McLain, 1977: Sea surface temperature related to rain in Ceara, northeast Brazil. *Nature*, **265**, 320–323.

Meehl, G. A., and H. Van Loon, 1979: The seesaw in winter temperatures between Greenland and Northern Europe. Part III: Teleconnections with lower latitudes. *Mon. Wea. Rev.*, **107**, 1095–1106.

Mossman, R. C., 1919: The rainfall of Fortaleza, Ceara, Brazil. *Quart. J. Roy. Meteor. Soc.*, **45**, 69–79.

Namias, J., 1972: Influence of Northern Hemisphere general circulation on drought in Northeast Brazil. *Tellus*, **24**, 336–343.

Pedlosky, J., 1979: *Geophysical Fluid Dynamics*. Springer-Verlag, 624 pp.

Ramos, R. P. L., 1975: Precipitation characteristics in the northeast Brazil dry region. *J. Geophys. Res.*, **80**, 1665–1678.

Ratisbona, C. R., 1976: The Climate of Brazil. *Climates of Central*

[2] All references in Portuguese, unless otherwise indicated, are available from: Instituto Nacional de Meteorologia (INEMET), Praca 15 de Novembro, 2 Sala 506, Rio de Janeiro, R.J., Brazil.

and South America, W. Schwerdtfeger and H. E. Landsberg, Eds., *World Survey of Climatology*, Vol. 12, Elsevier, 219–293.

Riehl, H., 1979: *Climate and Weather in the Tropics*. Academic Press, 611 pp.

Rose, N., 1980: A persisting misconception about the drought of 1958 in northeast Brazil. *Clim. Change*, **2**, 299–301.

Rowntree, P. R., 1976: Response of the atmosphere to a tropical Atlantic ocean temperature anomaly. *Quart. J. Roy. Meteor. Soc.*, **102**, 607–625.

Sampaio Ferraz, J. de, 1925: Causas provaveis das seccas do Nordeste brasileiro (Probable causes of droughts in Northeast Brazil). Ministerio da Agricultura, Diretoria de Meteorologia, Rio de Janeiro, 12 pp.

——, 1929: Sir Gilbert Walker's formula for Ceara's droughts: Suggestion for its physical explanation. *Meteor. Mag.*, **64**, 81–84.

——, 1950: Iminencia duma grande seca no Nordeste. (Imminence of a great drought in Northeast) Rev. Bras. Geogr., 12, 3–15.

Serra, A. B., 1945: Meteorologia do Nordeste Brasileiro (Meteorology of Northeast Brazil). IV Assembleia Geral do Instituto Pan-Americano de Geografia. Instituto Brasileiro de Geografia e Estatistica (IBGE), Rio de Janeiro.

——, 1956: As secas do Nordeste (The droughts in Northeast Brazil). Servico de Meteorologia, Ministerio da Agricultura, Rio de Janeiro, 28 pp.

——, 1973a: Aspectos estatisticos das secas nordestinas (Statistical aspects of Northeast Brazil droughts). Dept. Nacional de Meteorologia, Ministerio da Agricultura, Rio de Janeiro, 17 pp.

——, 1973b: Testes estatisticos para a previsao das secas nordestinas. (Statistical tests for Northeast Brazil drought forecasting). *Bol. Geogr.*, **32**, 78–104.

——, 1973c: Previsao das secas nordestinas (Forecasting of droughts in Northeast Brazil). Banco do Nordeste do Brasil, 55 pp.

——, and L. Ratisbona, 1942: As massas de ar da America do Sul (The air masses over South America). Servico de Meteorologia, Ministerio da Agricultura, Rio de Janeiro, 139 pp.

Shukla, J., 1975: Effect of Arabian sea-surface temperature anomaly on Indian summer monsoon: A numerical experiment with the GFDL model. *J. Atmos. Sci.*, **32**, 503–511.

——, and B. M. Misra, 1977: Relationships between sea surface temperature and wind speed over central Arabian sea, and monsoon rainfall over India. *Mon. Wea. Rev.*, **105**, 998–1002.

——, D. Straus, D. Randall, Y. Sud and L. Marx, 1981: Winter and Summer simulations with a GLAS General Circulation Model. NASA Tech. Memo. (to be published).

Smagorinsky, J., H. Riehl, J. Shukla, J. Rasmussen, J.O. Roads, S. Hastenrath, and W. M. Gray, 1980: Workshop on Drought Forecasting for Northeast Brazil—Panel Report. Brazilian National Research Council (CNPq), Institute for Space Research (INPE); Sao Jose dos Campos, Sao Paulo, February 11 to 15, 1980, 71 pp. [Available from INPE-C.P. 515; 12.200-Sao Jose dos Campos, S. P.; Brazil].

Strang, D. M. G. D., 1972: Analise climatologica das normais pluviometricas do Nordeste Brasileiro (Climatological analysis of rainfall normals in Northeastern Brazil). Centro Tecnico Aeroespacial, Relatorio Tecnico IAE-M-02/72, 70 pp. [Available from Centro Tecnico Aeroespacial/IAE; 12.200-Sao Jose dos Campos, S. P., Brazil].

——. 1979: Utilizacao dos dados pluviometricos de Fortaleza, CE, visando determinar probabilidades de anos secos e chuvosos (The use of Fortaleza, Ceara, rainfall data to determine probability of dry and wet years). Centro Tecnico Aeroespacial, Relatorio Tecnico ECA-03/79, 58 pp. [Available from Centro Tecnico Aeroespacial/IAE; 12.200-Sao Jose dos Campos, S. P.; Brazil].

Trewartha, G. T., 1961: *The Earth's Problem Climates*. The University of Wisconsin Press, 334 pp.

Walker, G. T., 1928: Ceara (Brazil) famines and the general air movement. *Beitr. Phys. Frein Atmos.*, **14**, 88–93.

Washington, W. M., and R. M. Chervin, 1980: Response time of an atmospheric general circulation model to changes in ocean surface temperature: Implications for interactive large-scale atmosphere and ocean models. *Tellus*, **32**, 119–123.

Webster, P. J., 1972: Response of the tropical atmosphere to local steady forcing. *Mon. Wea. Rev.*, **100**, 518–541.

Yamazaki, Y., and V. B. Rao, 1977: Tropical cloudiness over the south Atlantic ocean. *J. Meteor. Soc. Japan*, **55**, 205–207.